Front. Phys., 2014, 9(3): 323–350
DOI 10.1007/s11467-013-0408-7

REVIEW ARTICLE

Nanomaterials for electrochemical energy storage

Nian Liu[1], **Weiyang Li**[2], **Mauro Pasta**[2], **Yi Cui**[2,3,†]

[1] *Department of Chemistry, Stanford University, Stanford, CA 94305, USA*
[2] *Department of Materials Science and Engineering, Stanford University, Stanford, CA 94305, USA*
[3] *Stanford Institute for Materials and Energy Sciences, SLAC National Accelerator Laboratory, 2575 Sand Hill Road, Menlo Park, CA 94025, USA*
Corresponding author. E-mail: [†] *yicui@stanford.edu*
Received November 7, 2013; accepted December 5, 2013

The development of nanotechnology in the past two decades has generated great capability of controlling materials at the nanometer scale and has enabled exciting opportunities to design materials with desirable electronic, ionic, photonic, and mechanical properties. This development has also contributed to the advance in energy storage, which is a critical technology in this century. In this article, we will review how the rational design of nanostructured materials has addressed the challenges of batteries and electrochemical capacitors and led to high-performance electrochemical energy storage devices. Four specific material systems will be discussed: i) nanostructured alloy anodes for Li-batteries, ii) nanostructured sulfur cathodes for Li-batteries, iii) nanoporous open-framework battery electrodes, and iv) nanostructured electrodes for electrochemical capacitors.

Keywords nanomaterial, energy storage, silicon anode, sulfur cathode, stationary battery, electrochemical capacitors

PACS numbers 81.05.Rm, 82.45.Yz, 82.47.Aa, 82.47.Uv, 88.85.J-

Contents

1 Introduction

Today's globally growing efforts towards renewable and clean energy drive the urgent need for major breakthroughs in energy storage technology, which is critical in addressing the mismatched supply and demand in time and space associated with renewable energy sources [1]. Among various energy storage systems, electrochemical ones, such as rechargeable batteries and electrochemical capacitors (ECs), are especially attractive for

use in portable electronic devices (PEDs), electric vehicles (EVs), and grid-scale energy storage (GSES) [2, 3]. For portable applications such as in PEDs and EVs, higher volumetric (Wh/L) and gravimetric energy density (Wh/kg) are required. For stationary applications, such as GSES, lower capital cost ($/kWh/cycle life) is the key [4, 5].

The fundamental difference between batteries and ECs lies in the charge storage mechanism. A typical battery stores charges in the bulk of the electrodes through faradaic reactions, whereas a EC stores charges near the surface (electrochemical double-layer capacitance or redox pseudocapacitance). Hence, batteries have higher specific energy (Wh/kg), whereas ECs have higher specific power (W/kg). The former is useful when steady supply of energy is needed, while the latter finds applications where a burst of energy or high-frequency charge/discharge is needed, such as automotive regenerative braking and elevator operation.

The goal of higher energy density, faster kinetics, longer cycle life, improved safety and lower cost has always driven the development of electrochemical energy storage devices. Over the past two decades, nanostructured materials have been successfully applied in electrochemical energy storage devices, thanks to their unusual chemical, mechanical, and electrical properties endowed by confining the dimensions and combining the contribution of bulk and surface properties [6, 7]. This review covers four aspects of recent research in this area, most of which coming from our group: i) nanostructured high-capacity alloy anodes for Li-batteries, ii) nanostructured high-capacity sulfur cathodes for Li-batteries, iii) nanoporous open-framework battery electrodes, and iv) nanostructured electrodes for ECs.

2 Nanostructured high-capacity alloy anodes for Li-batteries

2.1 Opportunities and challenges for alloy anodes

State-of-the-art Li-ion batteries are composed of lithium metal oxide or phosphate cathodes and graphite anodes. To increase their energy density, electrode materials with higher capacity are needed. The graphite anode currently used in many devices today has a theoretical capacity of 372 mAh/g. Alloy anodes such as Si, Ge, and Sn offer much higher capacity. In particular, silicon has a theoretical capacity of 4200 mAh/g [8], more than ten times higher than graphite (Table 1). By simply replacing graphite with silicon, the full cell gravimetric energy density could have a 40% increase. This increase would be much higher if the conventional cathode is replaced by sulfur or oxygen-based cathodes [9]. The volumetric capacity of lithiated silicon, though severely expanded, still reaches 2370 mAh/cm^3, three times higher than lithiated graphite (Table 1). In addition to the higher capacity, the working potential of alloy anodes is slightly higher than graphite (Table 1), making the plating of lithium metal less likely to happen, thus improving the overal battery safety. Therefore, alloy anodes are promising for next generation Li-ion, Li-S, and Li-O_2 batteries.

The research on alloy anodes, in fact, started more than four decades ago [10, 11]. The main challenge that hinders their practical application is their colossal volume change upon cycling [12–14], which is not a problem for conventional graphite anodes (Table 1). Fundamentally different from the intercalation mechanism of graphite, alloy anode materials (A) break A-A covalent

Table 1 Comparison of the theoretical capacity, volume change, and potential of various anode materials.

Materials	Li	C	$Li_4Ti_5O_{12}$	Si	Ge	Sn
Density (g/cm^3)	0.53	2.25	3.5	2.3	5.3	7.3
Lithiated phase	Li	LiC_6	$Li_7Ti_5O_{12}$	$Li_{4.4}Si$	$Li_{4.4}Ge$	$Li_{4.4}Sn$
Density of lithiated phase (g/cm^3)	0.53	2.20	3.65	1.18	2.04	2.56
(ICDD PDF card number)	(00-001-1131)	(00-034-1320)	(00-049-0207)	(01-077-2882)	(00-017-0402)	(00-018-0753)
Theoretical specific capacity in delithiated state (mAh/g)	∞	372	175	4200	1620	993
Theoretical specific capacity in lithiated state (mAh/g)	3860	339	168	2010	1140	790
Theoretical volumetric capacity in delithiated state (mAh/cm^3)	∞	837	613	9660	8600	7250
Theoretical volumetric capacity in lithiated state (mAh/cm^3)	2050	747	614	2370	2330	2020
Volume change (%)	∞	12	1	410	370	260
Potential versus Li/Li$^+$ (V)	0	0.05	1.6	0.4	0.5	0.6

Notes:
1. Theoretical volumetric capacity = Theoretical specific capacity× Density
2. Volume change (%) = (Volume of lithiated phase ÷ Volume of delithiated phase –1) × 100

or metallic bonds, and form Li-A bonds. While this mechanism increases the number of Li that can be stored, it also results in colossal volume change of the host material. Silicon, for example, has a volume expansion as high as 410% upon lithiation, which causes a series of problems, including: i) material fracture and loss of active material during cycling [15, 16]; ii) electrode-level fracture and loss of electrical contact over the thickness of electrodes [17]; iii) unstable solid-electrolyte interphase (SEI) and its excessive formation [18]. These issues combined cause rapid capacity fading [19].

Starting from our pioneering work on Si nanowire anodes [20], rational structure design at the nanoscale has been successful in addressing the challenges of alloy anodes in the past several years [21]. By correlating nanostructure with function, we categorize the development into three generations: i) solid nano-Si (Ge, Sn), ii) hollow and porous nano-Si (Ge, Sn), and iii) clamped hollow nano-Si (Ge, Sn). Below we will review each of these categories, trying to summarize the underlying design principles.

2.2 Solid nano-Si (Ge, Sn)

In an early attempt to address the problems of silicon anodes, our group reported the nanowire anode design [Fig. 1(a)] [20] which shows three distinct advantages. First, unlike thick films and micron-sized particles, the diameters of the Si nanowires (Si NWs) are small (~100 nm), which enable the facile relaxation of the strain built up during Li insertion. Moreover, there are sufficient nanoscale empty spaces between Si NWs to accommodate their volume expansion. Second, the Si NWs are directly grown on stainless steel foil substrate via chemical vapor deposition (CVD), which guarantees a robust electrical and mechanical contact with the substrate. Third, the Si NWs form continuous 1D electron transport pathways across the thickness of the electrode, which allows all the Si materials to be electrochemically active, without the need of carbon additives or polymer binders. This is in contrast to the inefficient hopping of electrons between particles in traditional slurry-coated battery electrodes. These features result in significantly improved performance compared to previous studies: Si NW anode achieved initial delithiation capacity as high as 3124 mAh/g. Little capacity fading was observed over 10 cycles [Figs. 1(b) and (c)], which suggests the absence of active materials loss. The NW morphology preserves after cycling, without cracking, which further confirms the facile strain relaxation by the small diameter of NWs [Figs. 1(d) and (e)]. Later, we also demonstrated that Si NWs can be prepared by a more scalable supercritical fluid–liquid–solid method [22]. Ge and SnO_2 NW anodes have been later reported [23, 24].

It has been noticed, however, that the Si NW anodes experience capacity decay after 20 cycles of deep charge/discharge. We carried out solid-electrolyte interphase (SEI) [25], electrochemical impedance spectroscopy (EIS) [26], structural change [27], phase change [28] and porosity evolution [29] studies on Si NW anodes

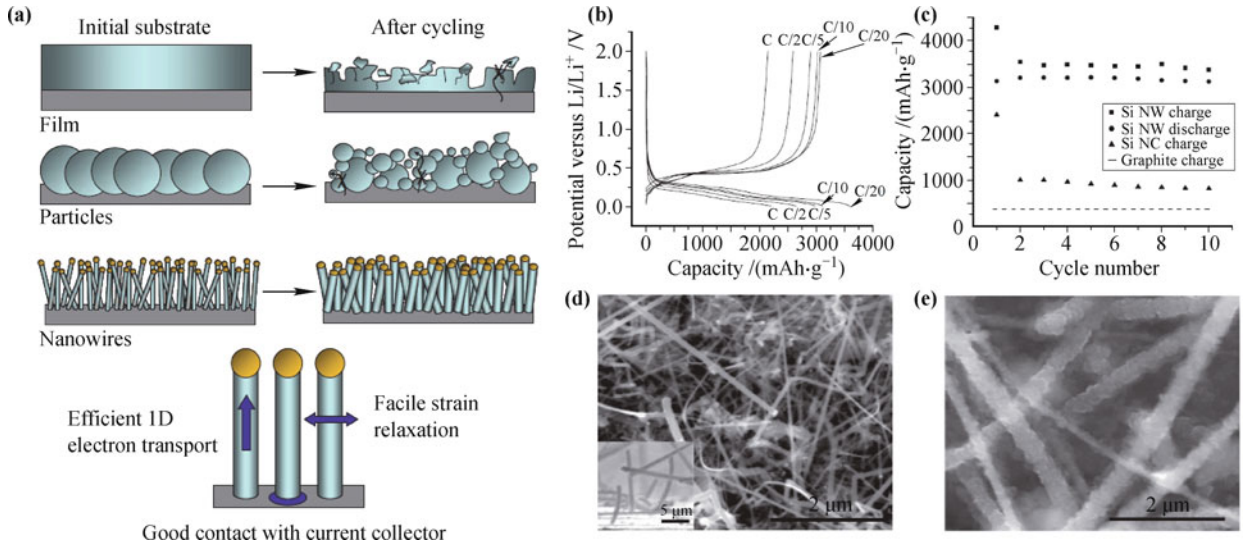

Fig. 1 **(a)** Schematic of morphological changes that occur in Si during electrochemical cycling. Due to the colossal volume change during cycling, Si films and particles tend to fracture during cycling. Much of the material loses contact with the current collector, resulting in capacity decay. Si NWs grown directly on the current collector do not break into smaller particles after cycling. Rather, facile strain relaxation in the NWs allows them to increase in diameter and length without breaking. **(b)** The voltage profiles for the Si NWs cycled at different rates. **(c)** Capacity versus cycle number for the Si NWs at the C/20 rate. **(d, e)** Scanning electron microscopy (SEM) images of Si NWs before (d) and after (e) cycling. Reproduced with permission [20], Copyright © 2008 Nature Publishing Group.

to identify the fading mechanism. Instead of cracking, the NWs become porous after cycling. Also, due to the higher surface area, electrolyte side-reactions and SEI formation on the NW surfaces are significant. In addition, the NWs decrease in mechanical strength upon cycling, which causes them to agglomerate. To extend the cycle life, our group designed carbon-silicon core-shell nanowires [30], in which amorphous silicon was coated onto carbon nanofibers (CNFs) to form a core-shell structure [Figs. 2(a) and (b)]. Since carbon has a much smaller capacity compared to silicon, the carbon core experiences less structural stress or damage during cycling and functions as a mechanical support and an efficient electron conducting pathway [Figs. 2(c) and (d)]. The resulted core-shell nanowires have a high capacity of ~2000 mAh/g and improved cycle life compared to Si NWs [Fig. 2(e)]. Using these core-shell nanowires, high mass loading and an area capacity of ~4 mAh/cm^2 were obtained, which are comparable to commercial battery values. Similar works have been done using silicon CVD coating on various inert nanostructured backbones including crystalline Si with controlled lithiation potential, Ni metal, metal carbide and metal silicide [31–35].

The surface coating of carbon [36, 37], copper [38], TiN [39] or conducting polymer [40], has also been found effective to prolong the cycle life of nano-Si. The coating has all or some of the following functions: i) enhances the electrical conductivity, ii) improves the mechanical integrity of the nanostructures, and iii) modifies the electrode/electrolyte interface [41]. The poly (3, 4-ethylenedioxythiophene) (PEDOT) coated Si NW anode, for example, can achieve 80% capacity retention after 100 cycles [40].

0D nanoparticles (NPs) are also capable of releasing the strain and prevent fracture. However, different from 1D NWs, maintaining the conductive pathway between particles over cycling is a challenge. The expansion and contraction of NPs results in dramatic shuffling and loss of electrical pathways. Since the conducting surfaces of the electrode exposed to the electrolyte is covered by insulating SEI after cycling, it is unlikely that the lost active material will reconnect electrically. Therefore, it is important not to lose the original electrical contact. Several approaches have been developed to realize this idea, such as inorganic glue [42], NPs embedded in NW forest [43], composite hierarchical structures [44, 45], and advanced polymer binders that strongly bind to Si NPs [46–48]. For example, we recently incorporated a conducting polymer hydrogel into Si NP-based anodes [49]: the polyaniline hydrogel is polymerized *in-situ*, resulting in a well-connected 3D network consisting of Si NPs conformally coated by the conducting polymer [Figs. 3(a)–(c)]. Such a hierarchical hydrogel framework provides a continuous conductive polyaniline network, which binds with the Si surface through either the crosslinker hydrogen bonding with phytic acid or the electrostatic interaction with the positively charged polymer. Moreover, the pores in the network allow to accommodate the volume expansion of Si. Such composite anode achieved 5000 cycles with over 90% capacity retention at a current density of 6.0 A/g [Fig. 3(d)].

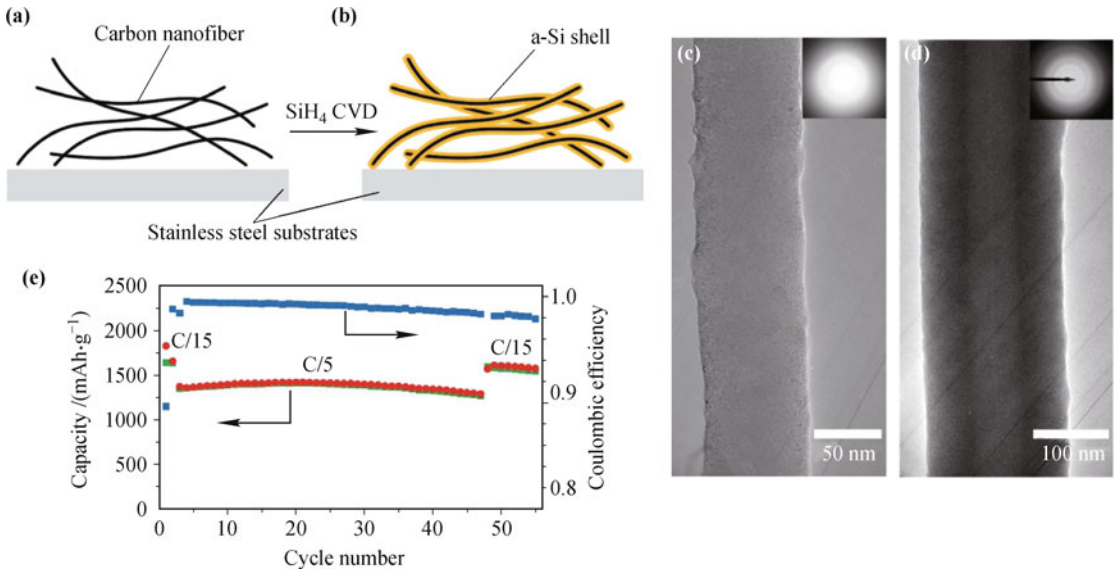

Fig. 2 **(a, b)** Schematic of Si CVD coating onto bare CNFs (a) to make C-Si core-shell NWs (b). **(c, d)** Transmission electron microscopy (TEM) and selected area electron diffraction (SAED) patterns (inset) of a bare CNF (c) and a C-Si core-shell NW (d). **(e)** Lithiation (*red*) and delithiation (*green*) capacity and Coulombic efficiency (CE, *blue*) versus cycle number for a half cell cycled between 0.1–1 V. Reproduced with permission [30], Copyright © 2009 American Chemical Society.

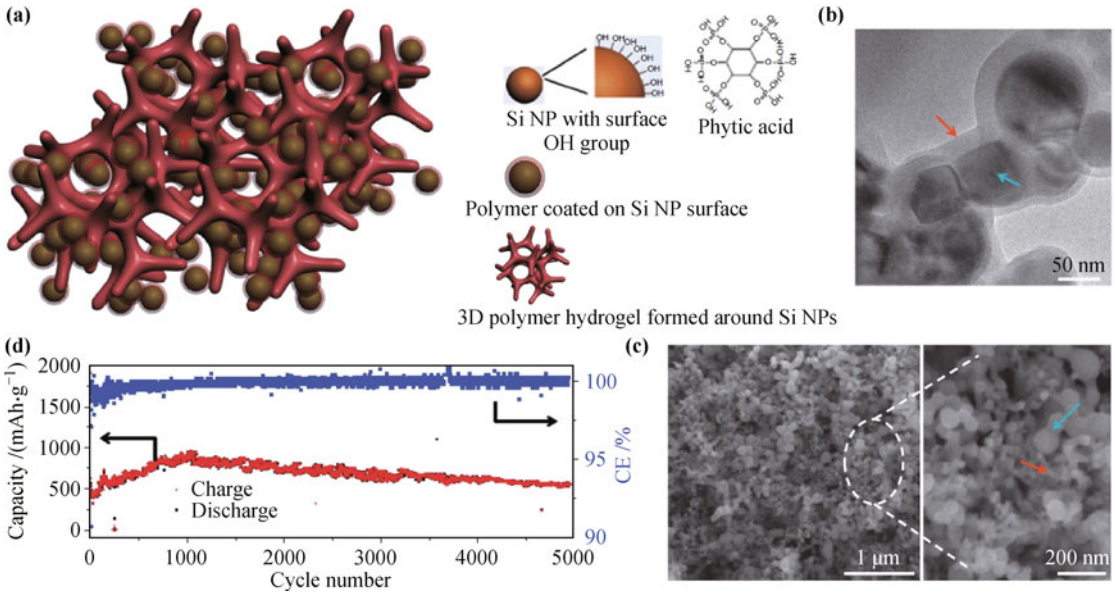

Fig. 3 **(a)** Schematic illustration of 3D porous Si NP/conductive polymer hydrogel composite electrodes. Each Si NP is coated by conductive polymer and is further connected to the highly porous hydrogel framework. **(b)** A TEM image showing the Si NPs (*blue arrow*) are coated with a uniform polyaniline (PAni) layer (*red arrow*). **(c)** SEM images of a Si NP-PAni composite electrode at low (*left*) and high (*right*) magnifications. The blue arrow indicates a Si NP while the red arrow shows the PAni hydrogel network. **(d)** Lithiation/delithiation capacity and CE of Si NP-PAni electrode cycled at current density of 6.0 A/g for 5000 cycles. Reproduced with permission [49], Copyright © 2013 Nature Publishing Group.

2.3 Hollow and porous nano-Si (Ge, Sn)

The demonstration of strain relaxation using solid nano-Si opened up the search for other nanostructures for alloy anodes, and motivated the synthesis of novel nanostructured Si, Ge, and Sn. Hollow structures, by definition, have internal empty spaces, which could effectively accommodate the volume expansion of alloy anodes. Indeed, this idea has been successfully demonstrated using Si nanotubes [50, 51], Si hollow nanospheres [52], Ge nanotubes [53], and SnO_2 hollow nanospheres [54, 55]. Si hollow nanospheres, for example, were fabricated using Si CVD templated by silica nanospheres and subsequent silica etching [Figs. 4(a) and (b)] [52]. Simulation shows that the maximum tensile stress (which can cause fracture) built up in a hollow Si nanosphere is five times lower than in a solid nanoparticle with an equal volume of Si. This advantage results in improved cycle life: less than 8% capacity degradation every hundred cycles for 700 total cycles was demonstrated [Fig. 4(c)]. Si hollow nanosphere electrodes also show a CE of 99.5% in later cycles.

An alternative way to introduce internal empty space is making Si nanoporous [56–62]. One of the methods to synthesis nanoporous Si is the reduction of nanoporous silica by Mg at around 650°C [63]. And various nanoporous silica can be rationally synthesized via sol-gel process [64, 65]. This relatively low temperature reaction usually retains the morphology of the silica counterparts and generates nanoporous Si. Using this method, recently we and two other groups have independently recovered nano-Si from rice husks, a major global agricultural byproduct with an annual yield of 1.2 million tons [66], and demonstrated its use as high-performance Si anode [67–69]. Such scalable, non-CVD production of nano-Si from sustainable source shows great promise for real application of Si anodes. Another scalable and facile method to produce nanoporous Si was recently demonstrated by disproportionation of SiO microparticles and subsequent etching of SiO_2 component. Assisted by a further carbon coating, stable cycling (600 cycles at 1200 mAh/g) and high tap density (0.78 g/cm^3) has been achieved [70].

2.4 Clamped hollow nano-Si (Ge, Sn)

Reducing the feature size of the active materials and engineering internal empty spaces have been successful in preventing the fracture and extending the cycle life of alloy anodes from tens to hundreds, by downsizing the feature size of the active materials in at least one dimension and creating internal empty spaces. To move forward from hundreds to thousands of cycles, another emerging challenge needs to be addressed: unstable solid-electrolyte interphase (SEI). As shown in Fig. 5(a), the electrolyte decomposes at the surface of anode due to the low chemical potential and forms a thin SEI during battery operation [71]. The SEI is electrically insulating

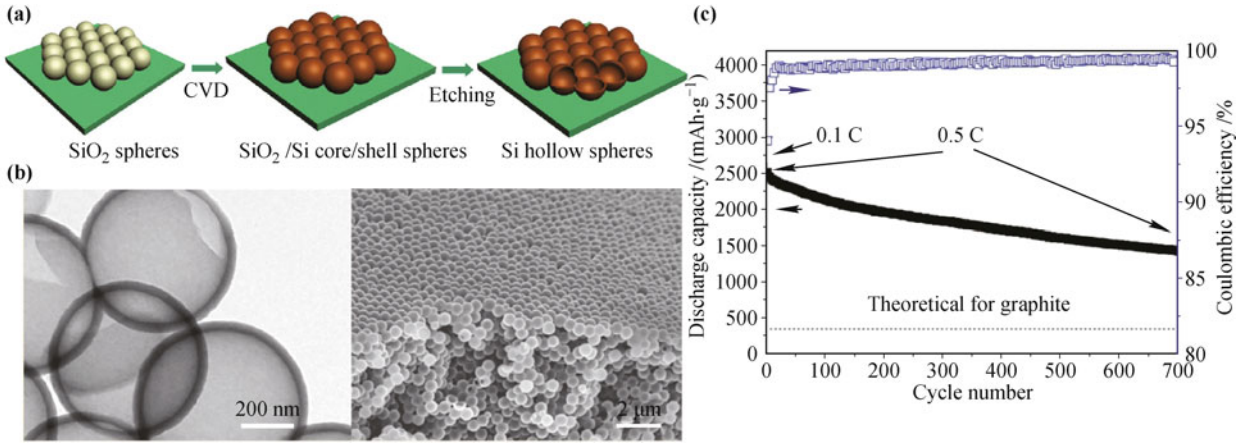

Fig. 4 **(a)** Schematic of Si hollow nanosphere synthesis. Silica particles (diameter ~175 nm) are first coated onto a stainless steel substrate, followed by CVD deposition of Si. The SiO_2 core is then removed by HF etching. **(b)** Typical TEM image and cross-sectional SEM image of Si hollow nanospheres. TEM image shows the hollow Si spheres are interconnected, with an inner diameter of 175 nm and outer diameter of 200 nm. **(c)** Reversible delithiation capacity (*black*) and CE (*blue*) versus cycle number for a half cell cycled between 0.01–1 V. The capacity degrades 8% per 100 cycles during the 700 total cycles. Reproduced with permission [52], Copyright © 2011 American Chemical Society.

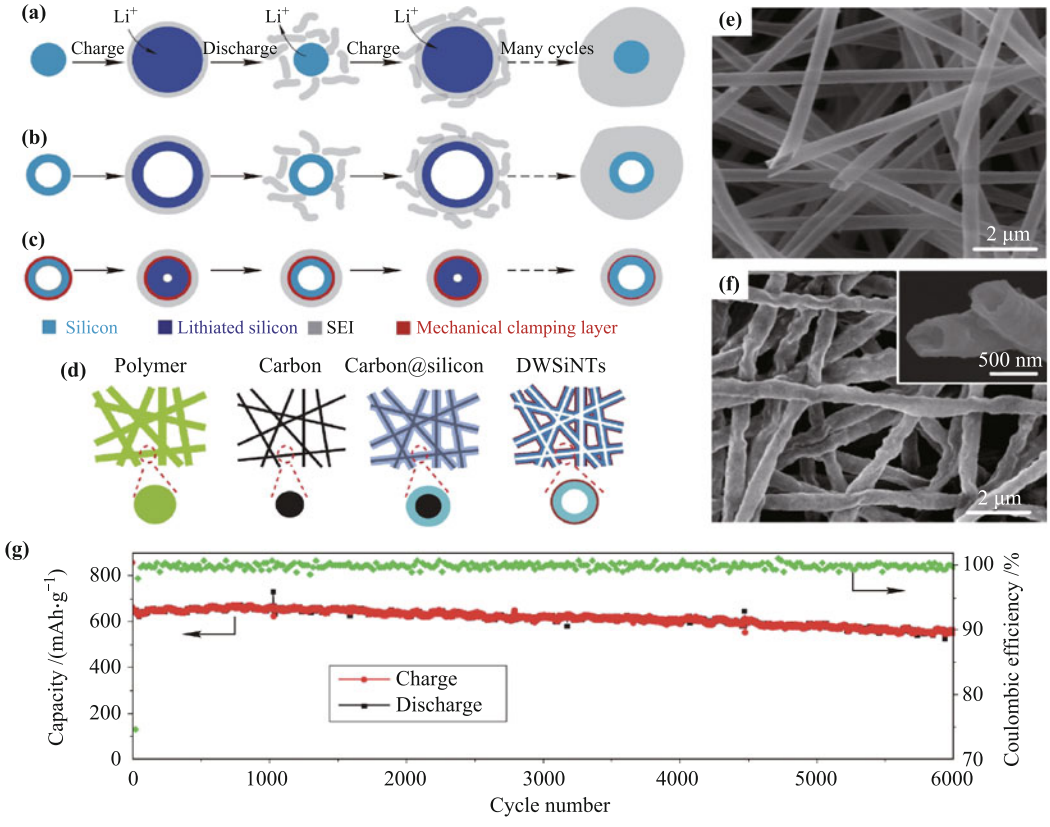

Fig. 5 **(a–c)** Schematic of SEI formation on Si surfaces. On a solid silicon nanostructure surface (a), SEI forms in the expanded state during lithiation, and breaks when silicon structures shrink during delithiation, exposing fresh silicon surface to the electrolyte. In later cycles, new SEI continues to form on the newly exposed silicon surfaces, which finally results in a very thick SEI layer outside. Similarly, a thick SEI grows outside the silicon nanotube without a mechanical constraining layer (b), which also has a varying and unstable interface with the electrolyte. Designing a mechanical constraining layer on the hollow silicon nanotubes (c) can prevent silicon from expanding outside towards the electrolyte during lithiation. As a result, a thin and stable SEI can be built. **(d)** Schematic of the fabrication process for DWSiNTs. **(e, f)** SEM images of DWSiNTs before (e) and after (f) 2000 cycles, showing the tubes coated with a uniform and thin SEI layer. **(g)** Lithiation/delithiation capacity and CE of DWSiNTs cycled at 12C for 6000 cycles. Reproduced with permission [19], Copyright © 2012 Nature Publishing Group.

but Li^+ can diffuse through [72]. SEI on conventional graphite anode is stable because of little volume change of graphite, but SEI on Si will break when Si contracts during delithiation, which exposes fresh silicon surfaces to the electrolyte and forms new SEI [73]. Such repetitive SEI disintegration and formation leads to a thick SEI on the surface, which not only consumes the electrolyte but eventually blocks the Li^+ diffusion and causes capacity fading. The accumulative thickening of the SEI determines that fading due to this mechanism can only be observed after the initial cycles. Hollow structure alleviates but does not solve this problem, because it still changes in outer dimension [Fig. 5(b)].

Our group recently reported a double-walled silicon nanotube (DWSiNT) anode structure to solve this problem [19]. Different from a simple Si nanotube, DWSiNT has a mechanical clamping layer on the outer surface [Fig. 5(c)], which forces the Si to expand towards the empty spaces inside upon lithiation, thus leaving the SEI outside stable and thin. To synthesize DWSiNTs [Fig. 5(d)], polymer nanofibres (green) were first made by electrospinning. The polymer fibres were then carbonized and coated with silicon (blue) by CVD. By heating the sample in air at 500°C, the inner carbon templates (black) were selectively removed, leaving continuous silicon tubes with a SiO_x mechanical constraining layer (red). These tubes have extremely high aspect ratios, so the electrolyte does not leak into the hollow regions. Furthermore, the SiO_x layer is Li^+ permeable, so the Si inside can still react while being clamped. The DWSiNTs have superior performance as anode. First, after as many as 2000 cycles, the SEI is still thin (~110 nm) and stable [Figs. 5(e) and (f)], which is not the case for solid and unclamped hollow nano-Si. Second, the DWSiNTs can cycle over 6000 times in half cells (12C, 600 mAh/g Si+SiO_x) while retaining more than 85% of their initial capacity [Fig. 5(g)], which is a big step forward. It has been noted that the SiO_x layer caused ~30% irreversible capacity in the first cycle, which could be addressed by performing prelithiation [74]. Apart from the structure design of the electrode, the unstable SEI problem can also be tackled by modification of the electrolyte [75, 76].

Other examples of clamped hollow nanostructures have been demonstrated for alloy anodes [78–83]. For example, our group has reported the novel "yolk-shell"

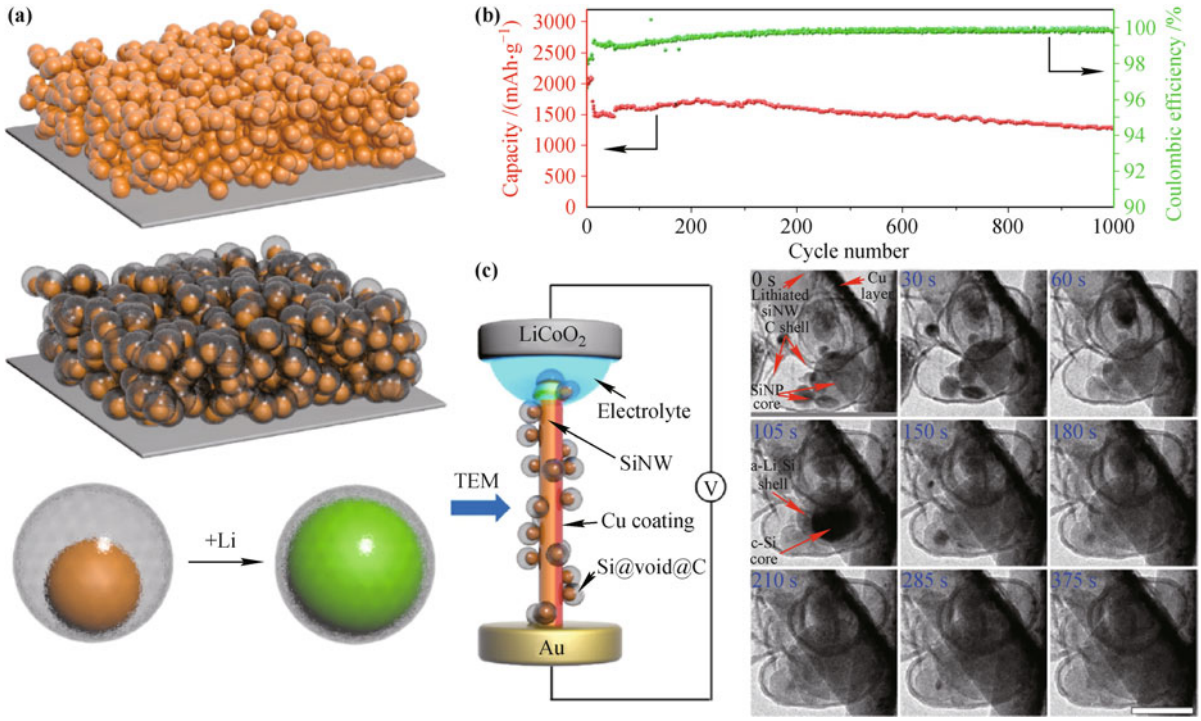

Fig. 6 **(a)** Schematic of the yolk-shell design. For a conventional slurry coated Si NP electrode (*top*), SEI on the surface of the Si NPs ruptures and reforms upon each Si NP during cycling, resulting in the excessive growth of SEI and failure of the battery. The expansion of each Si NP also disrupts the microstructure of the electrode. For the novel Si@void@C electrode (*middle and bottom*), the void space between each Si NP and the carbon coating layer allows the Si to expand without rupturing the coating layer, which ensures that a stable and thin SEI layer forms on the outer surface of the carbon. This mechanism also stabilizes the microstructure of the electrode. **(b)** Reversible delithiation capacity and CE of Si@void@C cycled at 1C for 1000 cycles. **(c)** *In situ* TEM characterization of Si@void@C expansion during electrochemical lithiation. The schematic of the device is shown on the left. The Si particles are observed to expand within the outer carbon shell. Scale bar: 200 nm. Reproduced with permission [77], Copyright © 2012 American Chemical Society.

alloy anode [Fig. 6(a)], in which commercially available Si NPs are completely sealed inside conformal, thin, self-supporting carbon shells, with rationally designed void space between the core and the shell [77]. The well-defined void space allows the Si NPs to expand freely without breaking the outer carbon shell, therefore stabilizing the SEI on the shell surface. Since the individual yolk-shell particles now internally accommodate the volume expansion of Si, the whole electrode will be stabilized as well and will not experience the shuffling and structural change as in the bare Si NP electrode. Hence, high capacity (2800 mAh/g at C/10), long cycle life (1000 cycles with 74% capacity retention), and high CE (99.84%) have been realized in this yolk-shell structured Si anode [Fig. 6(b)]. The successful design and fabrication is also confirmed by *in situ* TEM observation [84, 85] of our yolk-shell anode during lithiation [Fig. 6(c)]. The results show that Li indeed penetrates through the carbon shell and reacts with the Si core. And the Si core expanded inside the carbon shell without rupturing it.

The yolk-shell anode is attractive not only because it addresses the unstable SEI problem, but also because of its scalable/bulk fabrication process. And commercial Si NPs are the source, so no silane CVD was needed. Moreover, since the final product is in the form of powder, it is fully compatible with the slurry-coating industry manufacturing process.

3 Nanostructured high-capacity sulfur cathodes for Li-batteries

3.1 Background of lithium-sulfur battery and problems to be addressed

Lithium-sulfur (Li-S) batteries can significantly improve the state-of-the-art battery technologies due to its high specific energy density and low cost [9]. Sulfur, one of the most abundant elements on earth, is an exciting cathode material with a high theoretical specific capacity of 1673 mAh/g. In a Li-S battery, sulfur is reduced to lithium sulfide ($2Li + S \rightarrow Li_2S$) at an average potential of around 2.2 V, which results in a specific energy of around 2600 Wh/kg, six times higher than conventional Li-ion batteries based on metal oxide cathodes and graphite anodes [86]. Conventional Li-S battery is composed of a lithium metal anode, a multi-component organic liquid electrolyte, a porous separator, and a sulfur cathode consisting of micro-sized irregular shaped sulfur particles, carbon additives and polymer binder. Sulfur is usually in the form of cyclic octatomic molecules with the chemical formula S_8. During the discharge/charge process, sulfur undergoes a series of structural and morphological transformations, including the formation of electrolyte soluble lithium polysulfides (Li_2S_x, $4 \leqslant x \leqslant 8$) and insoluble Li_2S_2/Li_2S [86]. This operation mechanism leads to several problems that hinder the successful implementation of Li-S battery, preventing it from reaching the cycling performance suitable for portable electronics and electrical vehicles.

The poor cycle life of sulfur cathodes is a multifaceted issue which can be attributed to the following reasons [86–91]. i) The highly soluble intermediate lithium polysulfides can diffuse to the lithium anode, where they are reduced to insoluble Li_2S_2/Li_2S deposited on the anode surface, causing active material loss. Same reactions also occur on the cathode surface, where random deposition of Li_2S_2/Li_2S can drastically change the electrode morphology, resulting in inaccessibility of active materials and electrode degradation. This polysulfide diffusion also generates an internal redox shuttle, leading to low CE. ii) Large volume expansion (~80%) occurs when sulfur is reduced to Li_2S, causing significant stress in the electrode and aggravating the polysulfides diffusion as well. iii) Both sulfur and Li_2S are highly electrically and ionically insulating.

To address the challenges described above, an ideal structure for sulfur cathode should possess the following characteristics: i) a closed structure for efficient polysulfides confinement; ii) sufficient empty space to accommodate sulfur volumetric expansion (~80%); iii) small characteristic dimension of the sulfur to allow intimate contact with the electrically conductive materials and a short transport pathway for both electrons and lithium ions; iv) suitable electrolyte additives to passivate the lithium surface to minimize the shuttle effect. A variety of strategies have been developed to synthesize sulfur composites with favorable structures and properties to improve the cycling stability, specific capacity and CE of Li-S batteries [92–117]. In the following section we will review the recent developments on Li-S batteries mainly based on studies on sulfur cathode in our group.

3.2 Sulfur-carbon composite cathode and amphiphilic surface modification

Carbon has always been the focus of research as a conductive matrix or substrate to improve the electrochemical performances of Li-S batteries. Ever since the successful example of using highly ordered mesoporous carbon to constrain sulfur within its conductive channels in 2009 [92], a variety of carbon-based materials have been studied, including mesoporous hollow carbon spheres [93, 94], hollow/porous carbon nanofiber [95–97], activated car-

bon fiber [98], microporous carbon paper [99], acetylene black [100], highly porous carbon [101], and graphene oxide [102]. Our group has successfully designed and synthesized various nanostructured carbon-based sulfur composite electrodes to address the challenges associated with sulfur cathode [103–107]. Engineering the nanoscale architecture of the carbon matrix can be effective in achieving the dual goal of attenuating polysulfide dissolution and improving the overall electrode conductivity.

One notable structural design from our group is the hollow carbon nanofiber-encapsulated sulfur cathode [Fig. 7(a)] which demonstrated high specific capacity of 1400 mAh/g and excellent cycling stability [104]. The hollow carbon nanofiber arrays were fabricated using anodic aluminum oxide (AAO) templates through thermal carbonization of polystyrene. Sulfur was incorporated into the hollow carbon nanofiber arrays by heating a solution of sulfur in toluene with the carbon-coated AAO template. The AAO template was then etched away so that sulfur only coated on the inner wall of the carbon fibers. The high aspect ratio (200–300 nm in diameter and 60 μm in length) of the carbon nanofibers provides effective trapping of polysulfides, and the thin carbon wall allows rapid transport of lithium ions and electrons. The hollow structure also provides large space for sulfur expansion during cycling. A high specific capacity of ∼730 mAh/g was achieved at C/5 rate after 150 cycles of charge/discharge.

While hollow carbon nanostructured sulfur cathodes exhibited superior battery performance, their fabrication

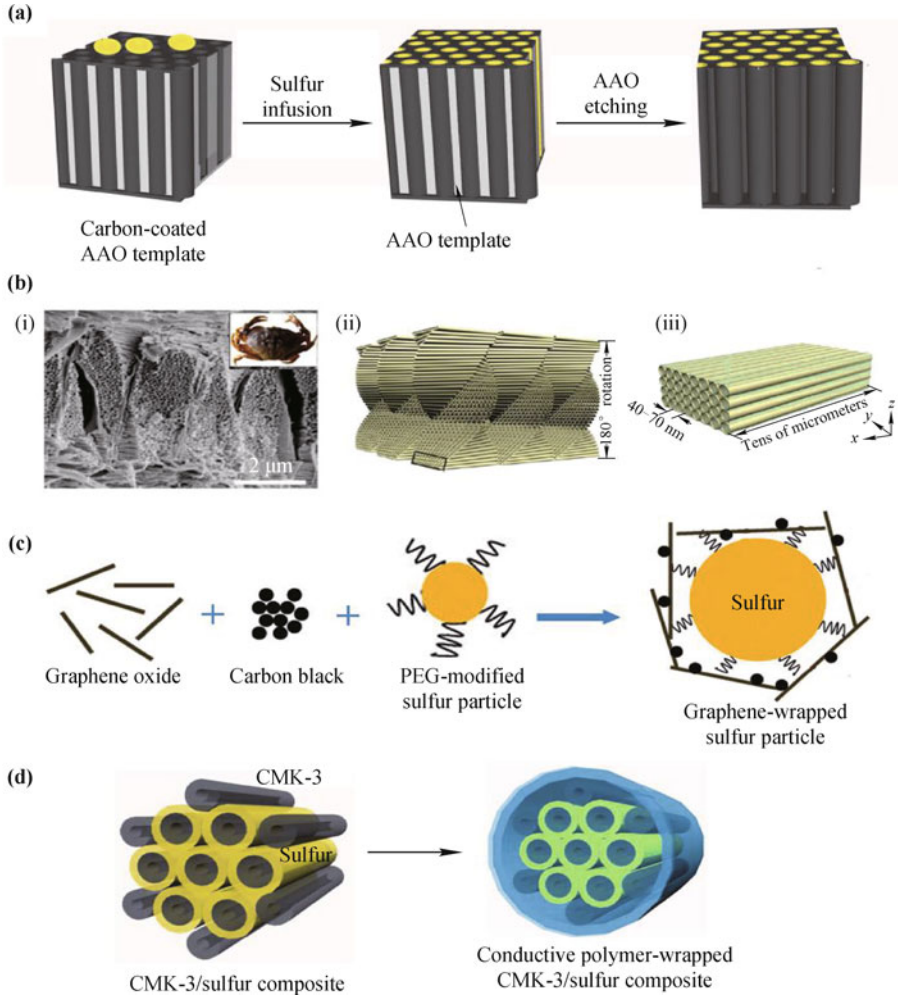

Fig. 7 **(a)** Schematic illustration of hollow carbon nanofiber-encapsulated sulfur cathode. Reproduced with permission [104], Copyright © 2011 American Chemical Society. **(b)** (i) SEM images of the biotemplates from a Dungeness crab, demonstrating the nanochannel arrays in crab shell templates. (ii) Structural model of twisted plywood nanochannel arrays in crab shell templates showing the hollow channels created by removing organic nanofibers in crab shells. (iii) Magnified image of the black square in (ii), showing the hollow channels arranged parallel to each other to form horizontal planes stacked in a helicoid fashion. Reproduced with permission [106], Copyright © 2013 American Chemical Society. **(c)** Schematic illustration of graphene-wrapped sulfur composite. Reproduced with permission [103], Copyright © 2011 American Chemical Society. **(d)** Schematic illustration of conductive polymer-coated mesoporous carbon (CMK-3)/sulfur composite. Reproduced with permission [107], Copyright © 2011 American Chemical Society.

often involves expensive starting materials and elaborate processing. Therefore, low-cost, scalable, and sustainable nanostructured templates are highly desirable for successful implementation of Li-S batteries. Recently our group demonstrated the use of crab shells consisting of mineralized chitin-protein fibers as biotemplates to fabricate hollow carbon nanofibers [Fig. 7(b)] [106]. As a sustainable natural resource, ~0.5 million tons of crab shell waste are generated every year from ~1.5 million tons of crab consumption. Crab exoskeletons consist of mineralized chitin-protein nanofibers containing bioceramic $CaCO_3$ in a twisted plywood pattern [118–121]. The chitin-protein organic components can be removed to form pure $CaCO_3$ frameworks containing nanochannels with an average diameter of ~70 nm. One piece of crab shell (15 g) can usually yield about 8 g of nanostructured $CaCO_3$. Carbon nanotube arrays were synthesized after a layer of carbon coating on the $CaCO_3$ frameworks which can then be dissolved away by acid. After infusing sulfur into these carbon nanotubes, the resulting sulfur cathode showed a high initial specific capacity of 1230 mAh/g and good cycling performance (up to 200 cycles with 60% capacity retention).

Other carbon-based nanostructured sulfur cathodes that have been developed in our laboratory include graphene-wrapped poly(ethylene glycol) (PEG)-coated sulfur particles [Fig. 7(c)] and conductive polymer-coated mesoporous carbon (CMK-3)/sulfur particles [Fig. 7(d)] [103, 107]. The strategy of using both carbon-based materials and polymer coatings in these two designs could provide double protection to trap soluble polysulfides. Both the graphene-sulfur composite and the conductive polymer-wrapped CMK-3/sulfur composite showed high and stable specific capacities up to 600 mAh/g over more than 100 cycles.

When carbon is used as the conductive matrix, rapid capacity decay of around 20%–30% in the first ten cycles is commonly observed. Although the formation of lithium polysulfides and their subsequent dissolution in the electrolyte has been suggested to account for the capacity decay observed in most Li-S batteries [108–110], this may not be the sole reason causing capacity decay. *In operando* transmission X-ray microscopy imaging on sulfur cathodes (made from commercial sulfur particles) indicated that dissolution of active materials into the electrolyte was not as severe as previously expected [111]. Therefore, mechanistic understanding of the sulfur cathode reaction from new perspectives is necessary.

In the *ex-situ* TEM study that was recently done by our group [105], we observed systematic delamination of discharged lithium sulfide from the carbon surface after sulfur lithiation [Fig. 8(a)], resulting in loss of electrical contact and capacity decay. To explain this observation, we carried out *ab initio* calculations to estimate the change in binding energy between sulfur and the carbon surface during the lithiation process. We found that there is a significant decrease in the chemical bonding between the carbon surface and the sulfur species after lithium reacts with sulfur. The binding energy between elemental sulfur atom and carbon is around 0.79 eV. The binding energy decreases to around 0.21 eV and 0.29 eV when one and two lithium atoms are added to the system, respectively [Fig. 8(b)], causing detachment of lithium sulfide from the carbon surface. The weakening of binding between the carbon and the discharged lithium sulfide can be tackled by introducing functional groups that have strong binding with both the carbon surface and lithium sulfides. We chose amphiphilic polymer, polyvinylpyrrolidone (PVP) to modify the carbon surface due to its strong binding with carbon surface from aqueous solution attributed to the strong thermodynamic driving force in eliminating the hydrophobic interface [122, 123]. Our simulation showed that lithium atoms in Li_xS ($0 < x \leqslant 2$) species can bind to the oxygen atom in PVP, giving high binding energies of 1.29 and 1.01 eV with LiS and Li_2S, respectively [Fig. 8(d)]. The TEM image of the discharged cathode did not show detachment of lithium sulfide from the carbon surface [Fig. 8(c)]. The modified sulfur cathode achieved stable performance of more than 300 cycles of charge/discharge with 80% capacity retention (a reversible capacity of ~650 mAh/g after 300 cycles) [Fig. 8(e)]. This study gave us important indications on the interfacial effect on the cycling stability of sulfur.

3.3 Monodisperse hollow and yolk-shell sulfur nanostructures

While encapsulating nanostructured sulfur to attenuate polysulfides dissolution and increasing the electrode conductivity have been the major areas of research for improving the Li-S battery performance, large volume expansion of sulfur is also a huge problem. Conventional core-shell sulfur nanostructures are not effective in trapping polysulfides, because the volume expansion of the sulfur core caused the protective layer to crack and fracture, aggravating the polysulfides dissolution. Engineering hollow space into sulfur nanostructures with coatings can effectively address this problem. In addition, for the fabrication of most carbon-based sulfur composites, sulfur needs to be melted and infused into the conductive matrix. Therefore, sulfur precipitation on the outer surface of the host matrix cannot be avoided. Additional processes are necessary to remove the inhomogeneously

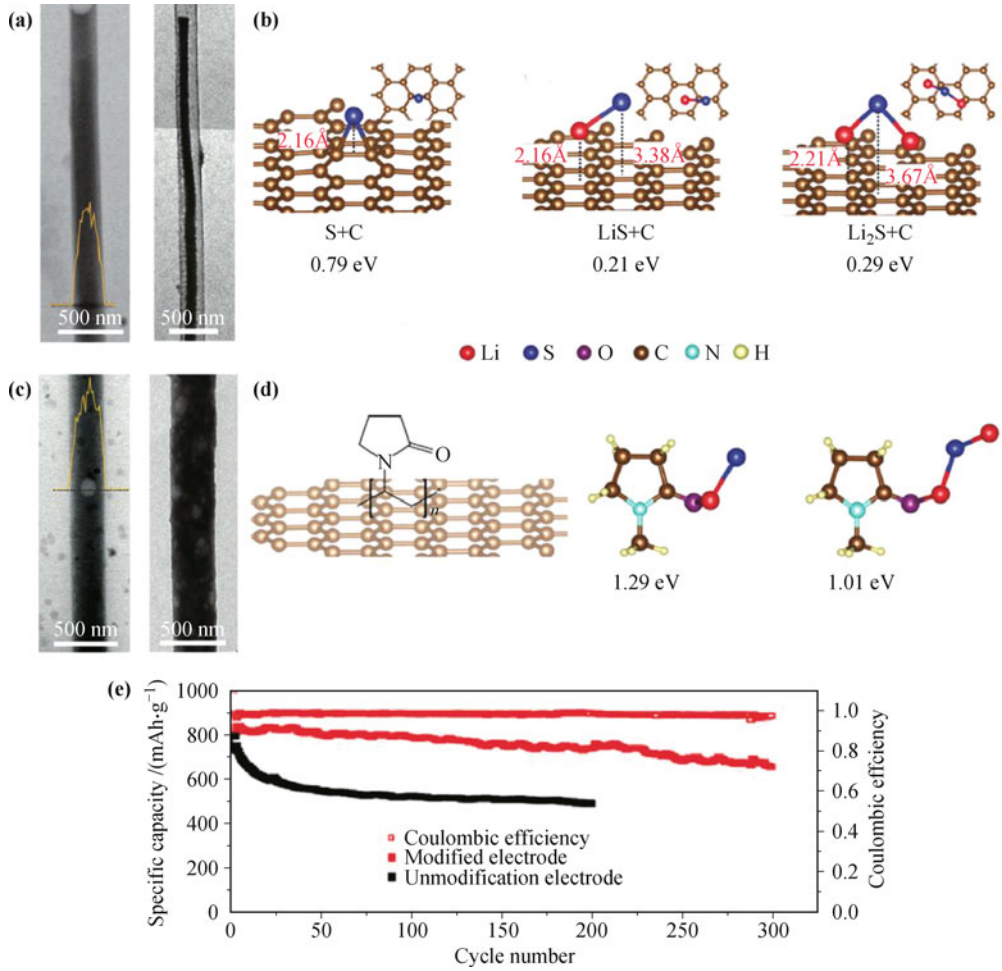

Fig. 8 **(a)** TEM image of the hollow carbon nanofiber encapsulated sulfur cathode (*left*) before discharge and (*right*) after fully discharge to 1.7 V. **(b)** First-principles calculations showing the interaction between the carbon surface and S, LiS, and Li_2S. The numbers represent the bond lengths between the sulfur atoms and the carbon surface in each case. The insets show the top views of the molecular configurations. **(c)** *left*: TEM image of the sulfur cathode after functionalization with polymer and infusion of sulfur. *right*: TEM image of the sulfur cathode after fully discharge. **(d)** Schematic showing the interaction between PVP and carbon surface, and first-principles calculation showing the interaction between the discharge products and the functional group on the polymer. **(e)** Comparison of cycling performance at C/2 with and without the PVP modification. Reproduced with permission [105], Copyright © 2013 American Chemical Society.

deposited sulfur [90, 104, 110]. This also leads to great variation in battery performance even with similar electrode structure and composition [103, 108, 114]. Tapping into the wet chemistry of nanoparticle synthesis offers great opportunities in manipulating the size and morphology of sulfur particles and thus provides unprecedented control over the electrode architecture from nanoscale to macroscale.

To realize a sulfur cathode that addresses all the above mentioned problems simultaneously, our group recently successfully demonstrated two rational designs of sulfur nanostructured cathode with tunable nanoscale morphology: monodisperse sulfur-TiO_2 yolk-shell nanoparticles and polymer-encapsulated hollow sulfur nanospheres [112, 113]. For the yolk-shell design [Fig. 9(a)], monodisperse solid sulfur nanoparticles were used as starting materials for the subsequent TiO_2 coating to form a core-shell nanostructure. Then the yolk-shell structures were fabricated by partially dissolving sulfur using toluene to create empty space between the sulfur core and the shell [Fig. 9(b)]. This internal void space can accommodate the volume expansion of sulfur without breaking the TiO_2 shell to greatly minimize the polysulfides dissolution. A similar concept was demonstrated for the polymer-encapsulated hollow sulfur nanospheres, while their fabrication was realized in a single-step, scalable, environmentally benign, room-temperature approach [Figs. 9(d)–(f)]. This represents a great advantage over the synthesis of sulfur-carbon composites and mesoporous oxides additives (mesoporous oxides were proved to be able to trap polysulfides) [89, 108, 114], which usually involves high-temperature process and highly

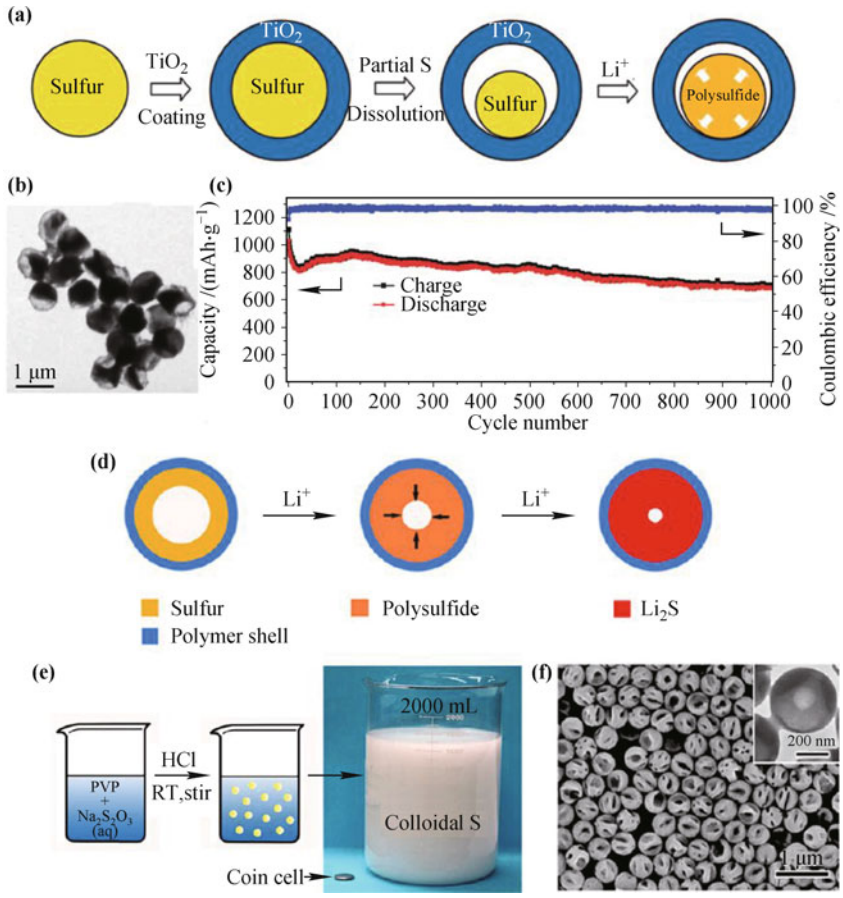

Fig. 9 **(a)** Schematic of the synthetic process that involves coating of sulfur with TiO_2 to form sulfur-TiO_2 core-shell nanostructures, followed by partial dissolution of sulfur in toluene to achieve the yolk-shell morphology. **(b)** TEM image of as-synthesized sulfur-TiO_2 yolk-shell nanostructures. **(c)** Charge/discharge capacity and CE of sulfur-TiO_2 yolk-shell nanostructures over 1000 cycles at C/2. Reproduced with permission [112], Copyright © 2013 Nature Publishing Group. **(d)** A Schematic showing the structure of PVP-encapsulated sulfur nanosphere with empty space inside and the inward expansion during lithiation for the accommodation of volume change and the confinement of polysulfides by the shell. **(e)** The fabrication process of PVP-encapsulated hollow sulfur nanospheres based on a simple reaction between sodium thiosulfate and hydrochloric acid in an aqueous solution in the presence of PVP at room temperature. Digital camera image of the synthesis scaled up in a 2000 mL beaker (on a scale of gram per batch). **(f)** SEM image of the hollow sulfur nanospheres after washing them with water to remove the PVP on the particle surface. Inset, TEM image of an individual hollow sulfur nanosphere. Reproduced with permission [113], Copyright © 2013 National Academy of Sciences, USA.

corrosive acid for template synthesis that significantly limits the manufacturability of the sulfur cathode materials. Using these highly uniform sulfur nanoparticles engineered with internal empty space and restraining shells, we demonstrated high specific capacities and excellent cycling stability. High initial specific capacities of ~1000 mAh/g at C/2 can be obtained. Over a long-term cycling of 1000 cycles at C/2, capacity decay as low as 0.033%–0.046% per cycle and an average CE of ~98.4% was achieved [Fig. 9(c)].

3.4 Lithium sulfide cathode: activation and bifunctional binder

Compared to sulfur, lithium sulfide (Li_2S) with a theoretical capacity of 1166 mAh/g also attracted much attention as promising cathode material because it can eliminate the requirement of lithium metal anode and use other less hazardous materials, such as silicon or tin, as alternatives [124–128]. This can avoid the safety concerns associated with metallic lithium including high reactivity and dendrite formation. The challenges of Li_2S cathode lie in the low conductivity and poor material utilization. Devising new methods to obtain nanostructured Li_2S and activate the highly insulating materials are crucial in realizing the full potential of Li_2S cathode. Our group developed the fabrication of CMK-3/Li_2S nanocomposite by chemically lithiating CMK-3/sulfur composite with *n*-butyllithium [Figs. 10(a) and (b)] [129]. The resulting Li_2S was confined within the tiny pores of CMK-3, leading to fast kinetics of the electrode reaction. The cell showed an initial capacity of 950 mAh/g (based on the

mass of Li_2S), which is about 30 times higher than that of commercial Li_2S particles. When paired with silicon nanowires anode, the full cell gave a high discharge capacity of 803 mAh/g at C/8 (146 mA/g), corresponding to a specific energy of 1050 Wh/kg based on the mass of active materials. Even at 1C, the full cell can still deliver a high capacity of 656 mAh/g.

While nanostructured Li_2S showed greatly improved electrochemical performances as cathode materials, the fabrication process is relatively complicated and not easy to scale up. Recently our group found out a facile method to activate the ball-milled, micrometer-sized Li_2S particles by applying a high charging cutoff voltage (~4 V) to overcome the initial potential barrier during the first charge [Figs. 10(c) and (d)] [130]. This leads to the formation of a polysulfide phase which drastically enhanced the kinetics of Li_2S. The activation barrier disappeared in the following cycling, and the battery showed similar electrochemical behaviors as common sulfur cathode. Using this activation approach, even for 10 μm-sized Li_2S, an initial capacity of over 800 mAh/g can be obtained, and a capacity of over 500 mAh/g can still be achieved after 50 cycles of charge/discharge.

Although the activation of Li_2S opens great opportunities for the utilization of commercially available Li_2S particles, Li_2S still retains the same problem of polysulfides dissolution as sulfur cathode. Enlightened by the binding between Li_2S and amphiphilic polymer in improving sulfur cathode performance described above, we used *ab initio* simulations to elucidate the interaction between Li_2S and lithium polysulfides with various functional groups in macromolecular binders [131]. Based on the simulation, we chose PVP as a dual-functional binder for Li_2S cathode. The PVP binder not only binds strongly with Li_2S to form a uniform dispersion of active material and carbon in the electrode slurry, but also shows strong binding affinity with lithium polysulfides to minimize their loss into the electrolyte during cycling [Figs. 10(e)–(h)]. A high discharge capacity of 760 mAh/g (based on the mass of Li_2S) was achieved at C/5 with stable cycling over 500 charge/discharge cycles (69% capacity retention) [Fig. 10(i)].

4 Nanoporous Prussian Blue analogues for stationary energy storage

4.1 Prussian Blue analogues (PBAs)

Prussian Blue, or ferric hexacyanoferrate, is one of the oldest known coordination complexes [132]. A whole family of materials has been named after it: Prussian Blue analogues (PBA). Their chemical formula can be represented by $A_xP_y\,[R(CN)_6]_z{\cdot}wH_2O$ (A is an alkali cation, and P and R are transition metal ions). These compounds exhibit a variety of interesting physical properties, including sensitivity to humidity [133], ion exchange [134], pressure-induced CN flipping [135], zero thermal expansion [136], hydrogen storage [137], novel magnetic properties [138–140] and chemical sensing [141]. The electrochemistry of electrodeposited thin films of PBAs has been extensively studied in the past for applications in electrochromism, beginning with Neff's pioneering works [140, 141]. The electrochemical behavior of PBAs is the result of the redox activity of one (or both) of the transition metal ions in the structure, accompanied by the insertion-extraction of alkali cations into/out of the lattice:

$$A_xP_y[R^{III}(CN)_6]_z + a(A^+ + e^-) = A_{x+a}P_y[R^{III}(CN)_6]_{z-a}[R^{II}(CN)_6]_a$$

In addition to the chemical formula, PBAs share a peculiar *open framework, nanoporous crystal structure* described in detail in the next section, which confers to this class of materials outstanding electrochemical properties. When operated in an appropriate aqueous electrolyte, PBA electrodes show extremely long cycle life, fast kinetics and high efficiency, making them ideal candidates for batteries used in grid-scale stationary energy storage applications.

4.2 The open framework nanoporous crystal structure

As shown in Fig. 11, PBAs exhibit a 3D host framework crystal structure and cubic nanopores with edge lengths of 5 Å [142]. This structure is composed of a face-centered cubic framework of transition metal cations where each cation is octahedrally coordinated to hexacyanometallate groups [143–145]. Both the P-site transition metal cation and the $R(CN)_6^{2-/3-}$ hexacyanometallate anion can be electrochemically active in this structure.

Large interstitial "A sites" within the structure can accommodate zeolitic water and alkali ions. The stoichiometry (y/z ratio) determines the $R(CN)_6$ vacancy concentration and the water content in PBAs. The alkali ions, water molecules, and $[R(CN)_6]$ vacancies constitute structural defects in PBAs and influence their physical properties [146]. This nanoporous, open framework structure fundamentally differs from that of other insertion electrode materials because of the large channels between the A sites that allow for rapid insertion and removal of both alkali and non-alkali ions. In addition, there is little lattice strain during cycling because

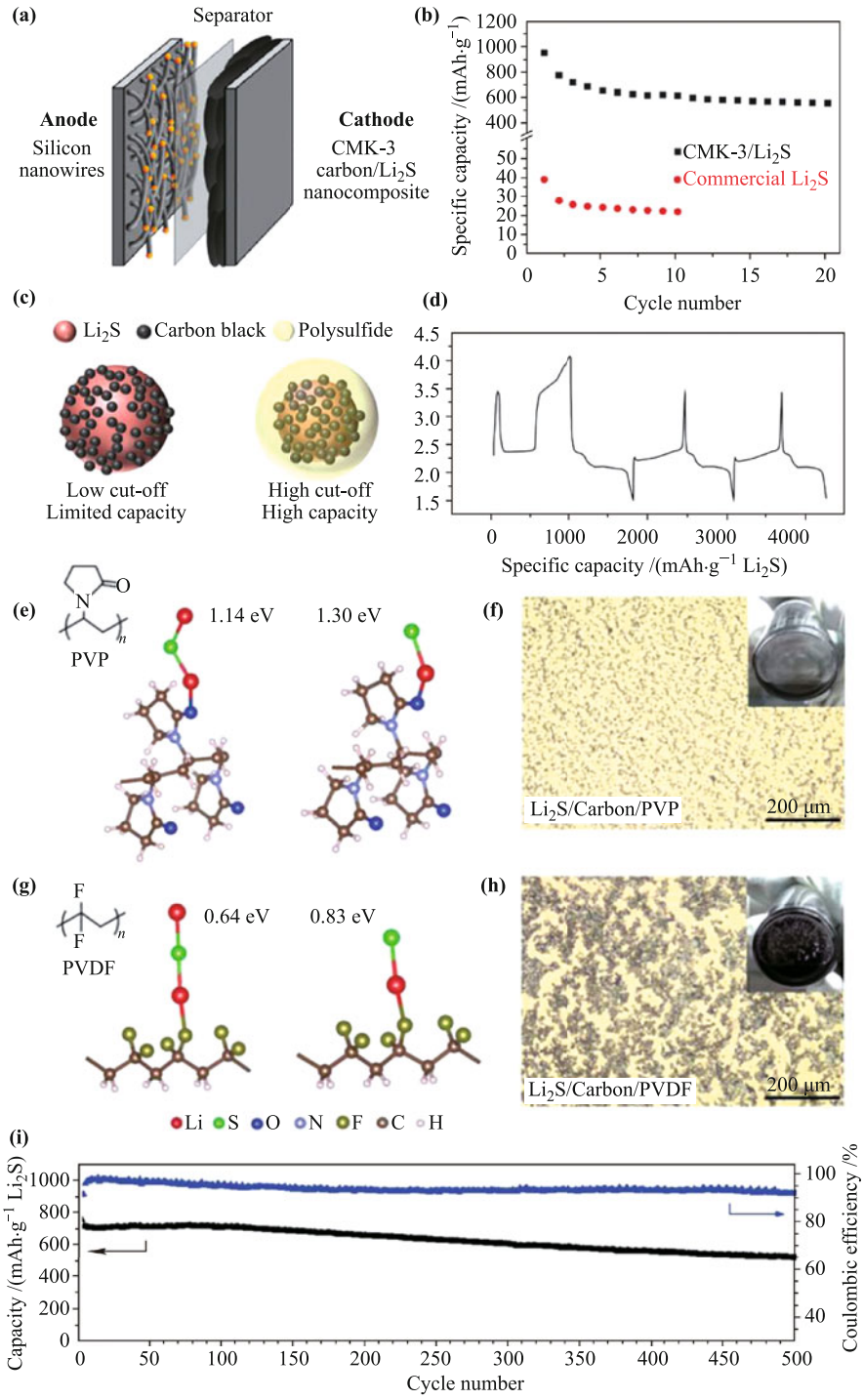

Fig. 10 **(a)** A schematic of a CMK-3 mesoporous carbon-embedded Li_2S/silicon nanowire battery. **(b)** The cycling performance of a CMK-3/Li_2S cathode compared to a commercial 10 μm-sized Li_2S particle electrode. Reproduced with permission [129], Copyright © 2010 American Chemical Society. **(c)** Schematic illustration of the effect of applying a high cutoff to activate Li_2S. After overcoming the initial barrier, a polysulfide phase is formed and Li_2S becomes active. **(d)** Voltage profile of a pristine Li_2S electrode in the initial three cycles. Potential barrier was observed only at the beginning of the first charge. Electrode was charged to 4.1 V vs. Li/Li^+ first and then cycled between 1.5 and 3.5 V. Reproduced with permission [130], Copyright © 2012 American Chemical Society. **(e, g)** *Ab initio* simulations showing the most stable configuration and calculated binding energies of Li_2S and Li-S· species with (e) PVP and (g) PVDF binders. **(f, h)** Optical microscopy and digital camera images (inset) showing the electrode slurry of (f) Li_2S/carbon black/PVP binder and (h) Li_2S/carbon black/PVDF binder in *N*-methyl-2-pyrrolidinone (60:35:5 by weight in both cases). **(i)** Specific capacity and CE of Li_2S cathodes using PVP binder upon prolonged cycling over 500 cycles at C/5. Reproduced with permission [131], Copyright © 2013 The Royal Society of Chemistry.

the A sites are larger than the ions that are inserted and removed from them [147]. This results in extremely stable electrodes: 10^7 cycles have been reported for Prussian Blue in electrochromic devices [148–150].

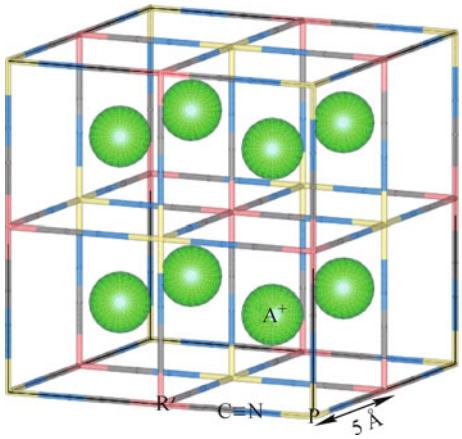

Fig. 11 The nanoporous, open framework crystal structure of PBAs in which transition metal ions (R-site is C coordinated while the P site is N coordinated) are linked by a face centered cubic framework of cyanide groups. In the case of CuHCF, octahedral hexacyanoferrate groups form a framework with six-fold nitrogen-coordinated copper. The framework contains large interstices, known as the "A Sites", which may contain zeolitic water or mobile, hydrated alkali ions. Each of the eight subcells of the unit cell contains a large "A site" that may be occupied by zeolitic water or hydrated alkali cations such as K^+ or Na^+. Hydrated ions may readily pass between one A Site and the next through channels in the ⟨100⟩ directions. This three-dimensional network of A Sites and channels allows for rapid transport of K^+ or Na^+ through the material without disturbance of the framework. Zeolitic water is omitted for clarity.

4.3 Electrolyte considerations

Most of the early studies on PBAs have focused on their aqueous electrochemistry [151]. It was not until recently that researchers started investigating their electrochemical properties in organic electrolytes with the goal of developing cathode materials for lithium-ion [152–158] and sodium-ion [159–163] batteries. Not only are electrolytes in aqueous batteries safer, more conductive, cheaper, and non-toxic [164], but the electrochemical performance of PBAs in organic electrolytes is also not nearly as impressive as in water in terms of cycle life, energy efficiency and power output. We believe that the differing behavior in organic versus aqueous electrolytes might be due to several reasons:

i) In aqueous electrolytes, alkali ions can be inserted in the open framework structure in their hydrated (or partially hydrated) form, while in organic electrolytes, the ions have to be fully desolvated before being inserted into the structure [165]. This results in suppressed activation energy for interfacial charge transfer in the case of hydrated ions [166] and therefore improved kinetics.

ii) The mechanism of ionic conductivity changes in different electrolytes. Water molecule ligands coordinate to the P ions adjacent to $[R(CN)_6]$ vacancies, and zeolitic water molecules reside in the A sites. The P ion acts as a Lewis acid, and a hydrated alkali ion is carried through the 3D hydrogen-bond network, which is composed of zeolitic and coordinated water molecules (Grotthus mechanism) [167].

iii) In organic electrolytes, the insertion of Li^+/Na^+ ions in the nanocubes and the concurrent reduction of transition metal ions result in a cooperative displacement of the alkali ions along the diagonal direction that destroys the macroscopic cubic symmetry, causing a rhombohedral distortion of the framework [168]. This process is hindered when, instead of the naked alkali ions, the bigger and charge-shielded hydrated alkali ions are inserted in the structure.

For all the above-mentioned reasons, we have decided to focus the efforts in our research group on electrodes for aqueous electrolytes.

4.4 PBAs in aqueous electrolyte batteries

Most of the early studies on PBAs have focused on the aqueous electrochemistry of hexacyanoferrates. In these materials the R-site is occupied by an electroactive Fe cation that changes its valence state between III and II upon charging/discharging. PBAs are known to be more stable at acidic pH than at neutral and basic pH, as ligand exchange between the CN^- ligands and OH^- ions results in the dissolution and destruction of the Prussian Blue structure [160]. The potential of hexacyanoferrates is close to 1 V versus standard hydrogen electrode (SHE), making them ideal cathode materials in a mildly acidic aqueous electrolyte. Different hexacyanoferrates have different potentials depending on both the nature of the transition metal ion in the P-site position [169] and the alkali ion inserted [170, 171] in the structure. Both effects have been quantitatively described by Dostal and Scholz in their 1996 paper [151]. Out of all the possible combinations, we have recently demonstrated that copper hexacyanoferrate ($K_xCu^{II}[Fe^{III/II}(CN)_6]$) is a very promising cathode material in sodium- and potassium-ion electrolytes. The material exhibits ultra-long cycle life (83% capacity retention after 40 000 cycles), high power (67% discharge capacity available at 80C), and high energy and Coulombic efficiencies (99.0% and 99.7%, respectively at C/6) [147]. We have later shown that nickel hexacyanoferrate ($Na_xNi^{II}[Fe^{III/II}(CN)_6]$) also exhibits a very long cycle life in a Na-ion electrolyte [172]. Another interesting property is that the reaction potential of

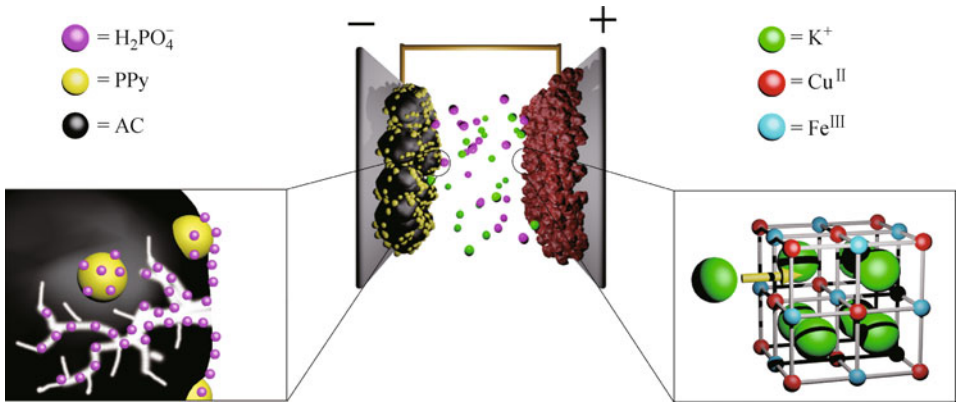

Fig. 12 Schematic of the full cell device. In the PPy/AC negative electrode (*left side*) the reduced PPy particles fix the open circuit potential close to the lower stability limit of the electrolyte while the charge is stored in the double layer built at the high surface activated carbon. The copper hexacyanoferrate (CuHCF) positive electrode (*right side*) has the nanoporous open framework structure. Reproduced with permission [173], Copyright © 2012 Nature Publishing Group.

copper-nickel hexacyanoferrate alloy nanoparticles may be tuned by controlling the ratio of copper to nickel in these materials [169].

These hexacyanoferrate cathodes are ideally paired with an anode that has comparable cycle life and kinetics to avoid a substantial constraint in the performance of the full battery. The activated charcoal used in commercial ultracapacitors has these properties, and we recently showed that a novel activated carbon/polypyrrole (PPy/AC) hybrid anode can be successfully combined with the $K_xCu^{II}[Fe^{III/II}(CN)_6]$ cathode in an asymmetric cell (Fig. 12) [173].

In the asymmetric cell, however, the low specific and volumetric capacity of capacitive electrodes severely limits the specific energy and energy density of the full cell. An ideal anode candidate is therefore another PBA with a lower potential, ideally close to 0 V versus SHE in order to maximize the 1.2 V electrochemical stability window of water. In order to achieve that, the electroactive ion in the structure needs to be replaced. Hexacyanometallates of Mn, Cr, Co, and Ru, among others, have long been studied for their magnetic and structural properties; however, their electrochemical properties have received very little attention. One exception is iron hexacyanoruthenate, also known as Ruthenium Purple, which is well-known for its electrochromic properties [158]. In 1995, Dostal and Scholz were the first to demonstrate the electrochemical activity of hexacyanomanganates and hexacyanochromates [159].

In particular, we have recently demonstrated the use of manganese hexacyanomanganate [159, 174, 175] ($Na_xMn^{II}[Mn^{III/II}(CN)_6]$) as an anode material that has a low reaction potential around 0 V versus SHE [176]. By combining this new anode with a copper hexacyanoferrate cathode, we demonstrate a new type of safe, fast, inexpensive, long-cycle-life aqueous electrolyte battery that relies on the insertion of sodium ions (Fig. 13). This high-rate, high-efficiency cell has a 96.7% round trip energy efficiency when cycled at a 5C rate and an 84.2% energy efficiency at 50C. There is zero capacity loss after 1000 deep-discharge cycles.

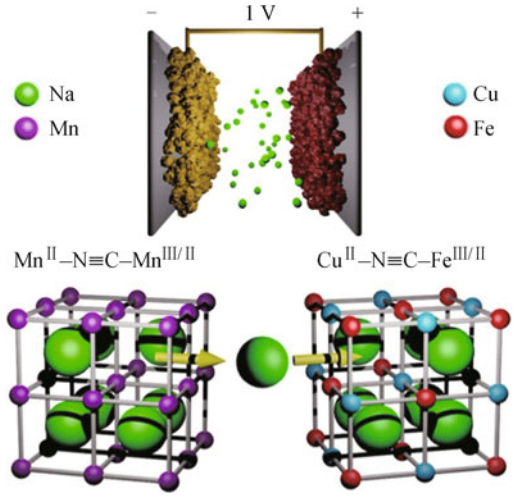

Fig. 13 Symmetric open framework cell schematic. This new type of safe, fast, inexpensive, long-cycle life aqueous electrolyte battery relies on the insertion of sodium ions into the copper hexacyanoferrate cathode and a newly developed manganese hexacyanomanganate anode, both of which have the same open framework crystal structure. Reproduced with permission [176], Copyright © 2014 Nature Publishing Group.

The main limitation of PBAs in aqueous electrolytes is their modest specific capacity of about 60 mAh/g, especially if compared with their theoretical specific capacity of more than 160 mAh/g. On the other hand, if synthesized with a low vacancy content and operated in an organic electrolyte, capacities of more than 120 mAh/g have been reported for manganese and cobalt hexacyanoferrate [159, 163]. This additional capacity derives from the electrochemical activity of the P-site transition metal

ions.

4.5 Other applications

The outstanding properties of PBAs are not only limited to aqueous batteries. Our research group is exploring their application in a variety of ambitious projects. The large A-site channels of the open framework crystal structure allow the insertion of not only monovalent alkali ions but also divalent alkaline earth and trivalent transition metal and rare earth cations [177]. Also, the ability to insert sodium ions and the very low solubility of PBAs in aqueous electrolytes make them ideal electrode materials for salinity difference devices previously developed by our research group, including mixing entropy [178] and desalination [179, 180] batteries. PBAs can be used as energy harvesting systems due to their usable specific entropy depending on the temperature. According to its high energy efficiency during charge and discharge process in aqueous electrolytes, the application of PBAs is expected to acquire highly efficient thermogalvanic systems.

5 Nanostructured electrodes for electrochemical capacitors

5.1 Introduction and basics

Apart from batteries, electrochemical capacitors (ECs) is another key electrochemical energy storage system [181]. In contrast to batteries' bulk storage mechanism through faradaic reactions, ECs take advantage of near-surface charge storage mechanisms (based on electrochemical double-layer capacitance or redox pseudocapacitance) to achieve much greater power density (1–2 orders of magnitude higher than batteries) [182]. The cycle life of ECs is typically measured in hundreds of thousands to millions of cycles, which is 2 to 3 orders of magnitude longer than batteries. These unique capabilities make ECs useful where a burst of energy needs to be generated or stored. Examples include automotive regenerative braking, elevator operation, uninterruptible power supplies (quickly bring the grid up to full power in seconds), and high-frequency electric grid load leveling [183].

The energy storage mechanism of ECs can be classified into: electrochemical double-layer capacitors (EDLCs) and pseudocapacitors [184]. EDLCs store charges electrostatically at the electrode/electrolyte interface, and usually use high surface area carbon-based materials as electrodes. Pseudocapacitors use fast and reversible redox reactions at the surface of electroactive materials to store charges, and use electrode materials of transition metal oxides such as RuO_2 [185, 186], MnO_2 [187], or conductive redox polymers such as polyanilines, and polypyrroles [188]. Pseudocapacitors typically have higher specific capacitance (300–1000 F/g) than EDLCs (100–250 F/g), at some cost of power density and cycle life.

Nanostructured materials as EC electrodes have several advantages, among which are short electron and ion transport path, large surface area between electrode and electrolyte, and new reactions that are not possible with bulk materials [6]. The disadvantages include potentially more complex synthesis and higher manufacturing cost. Below we will review works, mainly from our group, on EC electrodes using (a) conductive paper, textile and sponge, (b) nanostructured hybrid carbon-metal oxide, and (c) nanostructured conductive polymer hydrogel.

5.2 Conductive paper, textile, and sponge

Paper, invented more than 2000 years ago and widely used today in our everyday lives, actually has many advantageous properties as the support structure for ECs and batteries. First, paper is porous, which allows facile ion diffusion. Second, paper is lightweight, which increases the total energy density of the device. Third, paper is a renewable source with low cost and mature manufacturing. Fourth, the surface of paper is rich of –OH groups, which are easy to functionalize. Therefore, if paper can be modified to be conductive, its new era of applications in energy storage technologies will be opened [189]. Due to their large surface area and high conductivity, single-walled carbon nanotubes (SWNTs) have been regarded as attractive EDLC electrode material [190, 191]. Our group has demonstrated that commercially available paper can be made highly conductive with a sheet resistance as low as 1 ohm per square (Ω/sq) by using simple solution processes to achieve a conformal coating of SWNT film [Figs. 14(a)–(d)] [192]. Compared with plastic ones, paper substrates can improve the film adhesion, simplify the coating process, and lower the cost. EDLCs based on CNT-conductive paper show excellent performance [Figs. 14(e)–(h)]. When only CNT mass is considered, a specific capacitance of 200 F/g, a specific energy of 30–47 Wh/kg, a specific power of 200 000 W/kg, and a stable cycling life over 40 000 cycles are achieved. These values are much better than those of devices on other flat substrates, such as plastics. Even in a case in which the weight of all of the dead components is considered, a specific energy of 7.5 Wh/kg is achieved.

Apart from paper, we have also fabricated conductive

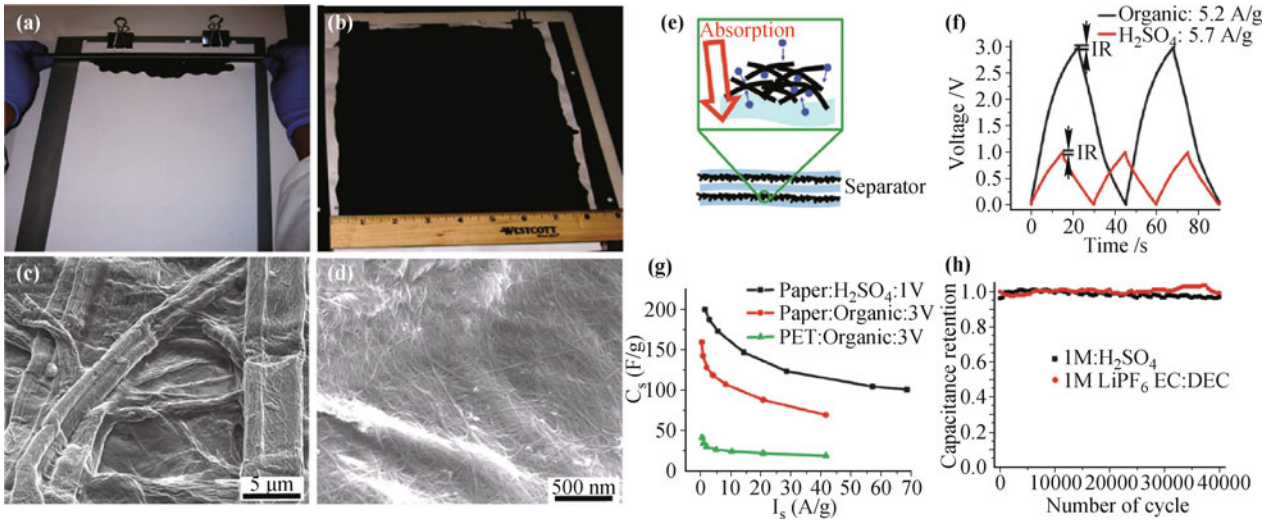

Fig. 14 **(a)** Meyer rod coating of CNT ink on commercial Xerox paper. **(b)** Conductive Xerox paper after CNT coating with sheet resistance of ∼10 Ω/sq. **(c, d)** SEM images of surface morphology of Xerox paper (c), and conformal CNT coating along fibers in Xerox paper (d). **(e)** Schematic illustration of all-paper ECs based on CNT conductive paper. Zoomed-in schematic illustrates that ion accessibility is enhanced by the strong solvent absorption. **(f)** Galvanostatic charging/discharging curves with 3 V and 1 V voltage window in organic and aqueous electrolyte, respectively. **(g)** Gravimetric capacitances at various currents measured in aqueous and organic electrolytes. Data from CNTs on polyethylene terephthalate (PET) are plotted together for comparison. **(h)** Capacitance retention measured in different electrolytes. After 40 000 cycles, 97% and 99.4% of initial capacitances are maintained for sulfuric acid and organic electrolytes, respectively. Reproduced with permission [192], Copyright © 2009 National Academy of Sciences, USA.

textile and sponge using similar "dipping and drying" process and demonstrated their high performance as EC electrodes and current collectors for other applications [193–195]. And to make the device even lighter, we have even integrated electrodes and separator into single sheet of commercial paper by coating CNT on both sides of the paper [196]. Our group has later shown that conducting paper can be also made by simple drawing on paper using graphite rods [197].

5.3 Nanostructured hybrid carbon-metal oxide

Metal oxides such as RuO_2 and MnO_2 have been attractive for ECs because of their high theoretical specific capacitance (1358 F/g for RuO_2 and 1370 F/g for MnO_2) enabled by the pseudocapacitance effect. MnO_2 is especially promising because of its low cost and environmental benignity. However, the main challenge for MnO_2 is its poor electrical conductivity ($\sim 10^{-6}$ S/cm). Forming hybrid structures with highly conductive materials has been effective for improved performance [198, 199]. Nanoporous gold substrate has been used to deposit MnO_2 to promote electron transport and ion diffusion [200], achieving a specific capacitance as high as 1145 F/g for MnO_2. However, to reduce the cost, conductive carbon materials are promising current collectors.

Utilizing the conductive CNT-textile as substrate, our group has reported the hybrid carbon-MnO_2 ECs [201]. Uniform MnO_2 particles with nanoflower morphology were deposited electrochemically onto CNT-textile. Even with a high MnO_2 loading of 8.3 mg/cm^2, the composite still maintained a porous structure. In an aqueous Na_2SO_4 (0.5 M) electrolyte, the highest specific capacitance achieved was 410 F/g, with a MnO_2 loading of 0.06 mg/cm^2 and a scan rate of 5 mV/s; while the highest areal capacitance obtained was 2.8 F/cm^2, at a high mass loading of 8.3 mg/cm^2 and a low scan rate of 0.05 mV/s. In comparison, MnO_2 deposited on Pt foil easily fractures even at a lower mass loading of 0.8 mg/cm^2. A similar study by another group using CNT-sponge as substrate demonstrated an even higher capacitance of 1230 F/g, which is very close to the theoretical limit, with a MnO_2 loading of 0.03 mg/cm^2 and a scan rate of 1 mV/s [202]. Their MnO_2-CNT-sponge ECs show only 4% of degradation after 10000 cycles at a charge/discharge specific current of 5 A/g. The specific power and energy of the MnO_2-CNT-sponge ECs are as high as 63 kW/kg and 31 Wh/kg, respectively.

To further reduce the cost for potentially large-scale energy storage systems, solution-exfoliated graphene has been explored to replace CNTs. Our group have demonstrated that solution-exfoliated graphene nanosheets (5 nm thick) can be conformally coated from solution on three-dimensional, porous textiles support structures achieving high loading of active electrode materials and facilitating the access of the electrolytes [Fig.

15(a)] [203]. With further electrodeposition of MnO_2 [Figs. 15(a)–(c)], the hybrid graphene/MnO_2-based textile yields a specific capacitance up to 315 F/g [Fig. 15(d)]. Moreover, asymmetric electrochemical capacitors with graphene/MnO_2-textile as the positive electrode and SWNTs-textile as the negative electrode in an aqueous Na_2SO_4 electrolyte solution were fabricated. These devices exhibit promising characteristics with a maximum power density of 110 kW/kg, an energy density of 12.5 Wh/kg, and excellent cycling performance (95% capacitance retention over 5000 cycles) [Fig. 15(e)].

The pseudocapacitor performance of graphene/MnO_2-based nanostructured electrodes can be further improved by a "3D conductive wrapping" method [204]. A small amount of CNTs or conducting polymers are coated onto graphene/MnO_2-based nanostructured electrodes by a simple "dipping and drying" process. After that, specific capacitance of the electrodes (considering the total mass of active materials) has substantially increased by ~20% and ~45%, respectively, achieving values as high as ~380 F/g. Moreover, these resulting electrodes have also exhibited excellent cycling performance with >95% capacitance retention over 3000 cycles. Such low-cost, high-performance energy textiles based on solution-processed graphene/MnO_2 hierarchical nanostructures offer great promise in large-scale energy storage applications.

5.4 Nanostructured conducting polymer hydrogel

Conducting polymers, such as polyaniline (PAni), polypyrrole (PPy), and polythiophene, have been investigated as electrode materials in energy storage devices for many years [188]. They are unique electroactive materials with large π-conjugation length and reversible redox and doping/dedoping reactions. Conducting polymers in the form of hydrogels have a high level of hydration and 3D microstructures, which promote the transport of charges, ions, and molecules [205]. As a result, conducting polymer hydrogels have demonstrated great potential for a broad range of applications from energy storage devices such as biofuel cells and ECs, to molecular and bioelectronics [206] and medical electrodes [207]. The synthesis of conductive polymer hydrogels often involves the polymerization of a conductive polymer monomer within a nonconducting hydrogel matrix, resulting in deterioration of their electrical properties [208–210].

Our group has recently reported a scalable and versatile synthesis of multifunctional polyaniline (PAni) hydrogel with excellent electronic conductivity and electrochemical activities (Fig. 16) [211]. Phytic acid, an

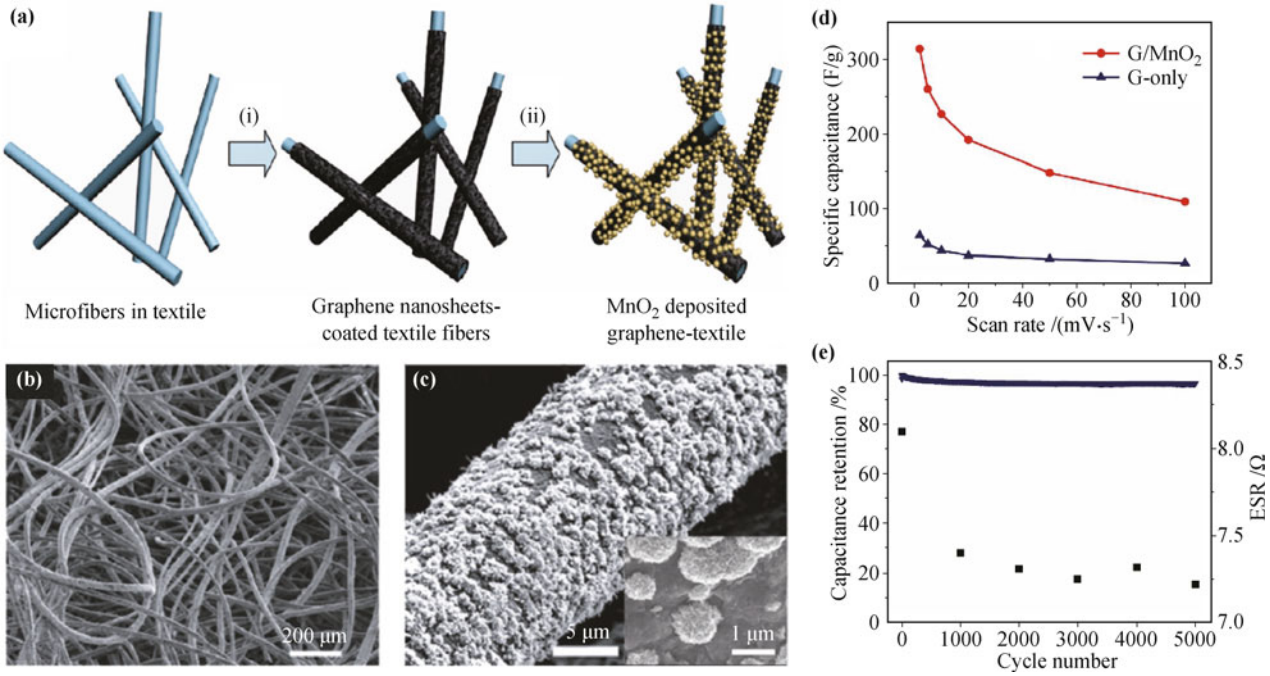

Fig. 15 **(a)** Schematics of the fabrication of hybrid graphene/MnO_2-nanostructured textiles as high-performance EC electrodes. **(b)** SEM image of a sheet of graphene-coated textile after MnO_2 electrodeposition. **(c)** Magnified SEM image of one microfiber in panel (b). *Inset*: Further magnified SEM image showing the nanoflower structure of electrodeposited MnO_2 particles. **(d)** Comparison of specific capacitance values between graphene/MnO_2-textile and graphene nanosheets-only textile at different scan rates. **(e)** Cycling performance of asymmetric ECs (graphene/MnO_2-textile as positive electrode, CNT textile as negative electrode) showing capacitance retention of ~95% after 5000 cycles of charging and discharging at a current density of 2.2 A/g, and subtle change in EC's equivalent series resistance (ESR) taken from impedance measurement every 1000 cycles. Reproduced with permission [203], Copyright © 2011 American Chemical Society.

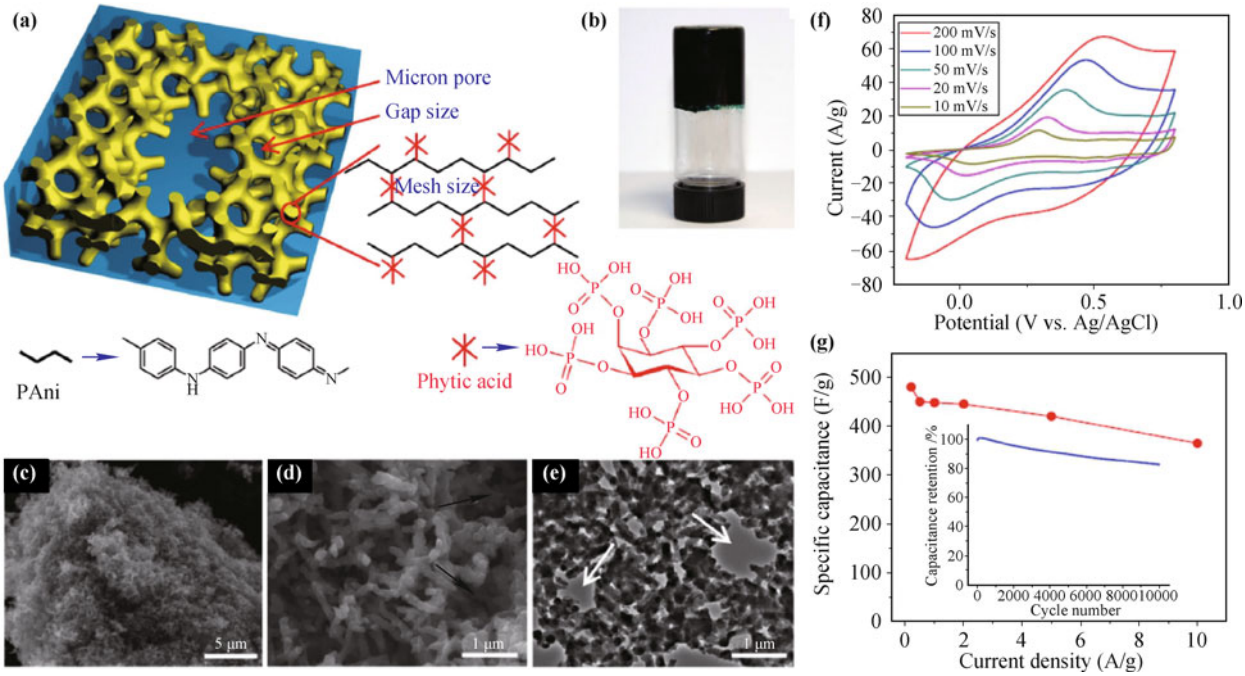

Fig. 16 **(a)** Schematic illustration of the 3D hierarchical microstructure of the gelated PAni hydrogel where phytic acid acts as both dopant and crosslinker. Three levels of hierarchical porosity from angstrom, nanometer to micron size pores have been highlighted by red arrows. **(b)** A photograph of the PAni hydrogel inside a glass vial. **(c)** SEM image of dehydrated PAni hydrogel. **(d)** A magnified SEM image showing the interconnected network of dendritic PAni nanofibers. **(e)** A TEM image showing the continuous nanostructured network of the dehydrated PAni hydrogel. The white arrows in (d) and (e) denote the micron-sized pores in PAni hydrogel. **(f)** Cyclic voltammogram curves of the PAni hydrogel electrode at different scan rates (10–200 mV/s). **(g)** Summary plot of specific capacitance values vs. current density for PAni hydrogel electrodes. *Inset*: Cycling test showing ~83% capacitance retention over 10 000 cycles at high current rate of 5 A/g. Reproduced with permission [211], Copyright © 2012 National Academy of Sciences, USA.

abundant natural product found in plants, was used as the gelator and dopant to directly form a conducting polymer network free of insulating polymers [Figs. 16(a) and (b)]. The PAni hydrogels with phytic acid gelator showed a new record conductivity of 0.11 S/cm among several conducting polymer hydrogels reported to date. And with their unique features of high surface area and 3D porous nanostructures [Figs. 16(c)–(e)], the PAni hydrogels demonstrated potential as high-performance EC electrodes with high specific capacitance (~480 F/g), unprecedented rate capability, and cycling stability (~83% capacitance retention after 10 000 cycles) [Figs. 16(f) and (g)].

Due to their excellent conductivity and 3D hierarchical porous structure, the PAni hydrogels have later been reported useful as glucose enzyme sensors and support structure for Li-ion battery high-capacity electrodes [49, 211, 212].

6 Conclusion and perspective

This review demonstrates how nanomaterials can significantly change electrode properties, and consequently their performance in electrochemical energy storage devices. In some cases the effects may be simple consequences of a reduction in size, for example higher tolerance of strain without fracture, and better kinetics due to higher electrode/electrolyte contact areas. In others the effects may be more complex, involving integrated consideration of many factors, for example the SEI control through double-walled Si nanotubes and yolk-shell structure. Apart from performance improvement, nanostructured materials coupled with nanoscale instrumentation have also led to new scientific understanding of the electrochemical processes. This opens up new opportunities for rational design of high-performance electrochemical energy storage systems using nanomaterials.

Looking forward, the specific challenges that need to be addressed are: Si anodes need further improvement on first cycle Coulombic efficiency, areal mass loading, overall volumetric capacity, and low cost and scalable fabrication, without sacrificing the achieved long cycle life; sulfur cathodes need further improvement on active material utilization, electrical conductivity, Coulombic efficiency, and accommodation of volume expansion; nanoporous open-framework batteries need improvement mainly on specific capacity; and EC electrode materials

need improvement on the energy density at high current density, and low fabrication cost.

Finally, in a more general overview, we do observe these changes in the research of nanomaterials in electrochemical energy storage in the past decade: i) The research is leaning towards property-oriented rather than structure-oriented. The most recognized nanomaterials are usually those endow the most desired properties; ii) Materials systems previously thought inapplicable could be made possible though nanotechnology; iii) Rational design gradually replacing undirected exploring.

Acknowledgements Y. Cui acknowledges the funding support from US Department of Energy, Global Climate and Energy Projects at Stanford University, US Office of Naval Research and King Abdullah University of Science and Technology over the years. M. Pasta acknowledges the support of the Oronzio and Niccolò De Nora Foundation.

References

1. S. Chu and A. Majumdar, Opportunities and challenges for a sustainable energy future, *Nature*, 2012, 488(7411): 294
2. J. M. Tarascon and M. Armand, Issues and challenges facing rechargeable lithium batteries, *Nature*, 2001, 414(6861): 359
3. M. Armand and J. M. Tarascon, Building better batteries, *Nature*, 2008, 451(7179): 652
4. Z. Yang, J. Zhang, M. C. W. Kintner-Meyer, X. Lu, D. Choi, J. P. Lemmon, and J. Liu, Electrochemical energy storage for green grid, *Chem. Rev.*, 2011, 111(5): 3577
5. B. Dunn, H. Kamath, and J. M. Tarascon, Electrical energy storage for the grid: A battery of choices, *Science*, 2011, 334(6058): 928
6. A. S. Aricò, P. Bruce, B. Scrosati, J. M. Tarascon, and W. van Schalkwijk, Nanostructured materials for advanced energy conversion and storage devices, *Nat. Mater.*, 2005, 4(5): 366
7. Y. G. Guo, J. S. Hu, and L. J. Wan, Nanostructured materials for electrochemical energy conversion and storage devices, *Adv. Mater.*, 2008, 20(15): 2878
8. W. J. Zhang, A review of the electrochemical performance of alloy anodes for lithium-ion batteries, *J. Power Sources*, 2011, 196(1): 13
9. P. G. Bruce, S. A. Freunberger, L. J. Hardwick, and J. M. Tarascon, Li-O_2 and Li-S batteries with high energy storage, *Nat. Mater.*, 2012, 11(1): 19
10. A. N. Dey, Electrochemical alloying of lithium in organic electrolytes, *J. Electrochem. Soc.*, 1971, 118(10): 1547
11. B. A. Boukamp, All-solid lithium electrodes with mixed-conductor matrix, *J. Electrochem. Soc.*, 1981, 128(4): 725
12. T. D. Hatchard and J. R. Dahn, *In situ* XRD and electrochemical study of the reaction of lithium with amorphous silicon, *J. Electrochem. Soc.*, 2004, 151(6): A838
13. M. N. Obrovac and L. Christensen, Structural changes in silicon anodes during lithium insertion/extraction, *Electrochem. Solid-State Lett.*, 2004, 7(5): A93
14. M. T. McDowell, S. W. Lee, W. D. Nix, and Y. Cui, 25th anniversary article: Understanding the lithiation of silicon and other alloying anodes for lithium-ion batteries, *Adv. Mater.*, 2013, 25(36): 4966
15. L. Y. Beaulieu, K. W. Eberman, R. L. Turner, L. J. Krause, and J. R. Dahn, Colossal reversible volume changes in lithium alloys, *Electrochem. Solid-State Lett.*, 2001, 4(9): A137
16. S. W. Lee, M. T. McDowell, L. A. Berla, W. D. Nix, and Y. Cui, Fracture of crystalline silicon nanopillars during electrochemical lithium insertion, *Proc. Natl. Acad. Sci. USA*, 2012, 109(11): 4080
17. J. H. Ryu, J. W. Kim, Y. E. Sung, and S. M. Oh, Failure modes of silicon powder negative electrode in lithium secondary batteries, *Electrochem. Solid-State Lett.*, 2004, 7(10): A306
18. J. O. Besenhard, J. Yang, and M. Winter, Will advanced lithium-alloy anodes have a chance in lithium-ion batteries? *J. Power Sources*, 1997, 68(1): 87
19. H. Wu, G. Chan, J. W. Choi, I. Ryu, Y. Yao, M. T. McDowell, S. W. Lee, A. Jackson, Y. Yang, L. Hu, and Y. Cui, Stable cycling of double-walled silicon nanotube battery anodes through solid-electrolyte interphase control, *Nat. Nanotechnol.*, 2012, 7(5): 310
20. C. K. Chan, H. Peng, G. Liu, K. McIlwrath, X. F. Zhang, R. A. Huggins, and Y. Cui, High-performance lithium battery anodes using silicon nanowires, *Nat. Nanotechnol.*, 2008, 3(1): 31
21. H. Wu and Y. Cui, Designing nanostructured Si anodes for high energy lithium ion batteries, *Nano Today*, 2012, 7(5): 414
22. C. K. Chan, R. N. Patel, M. J. O'Connell, B. A. Korgel, and Y. Cui, Solution-grown silicon nanowires for lithium-ion battery anodes, *ACS Nano*, 2010, 4(3): 1443
23. C. K. Chan, X. F. Zhang, and Y. Cui, High capacity Li ion battery anodes using Ge nanowires, *Nano Lett.*, 2008, 8(1): 307
24. P. Meduri, C. Pendyala, V. Kumar, G. U. Sumanasekera, and M. K. Sunkara, Hybrid tin oxide nanowires as stable and high capacity anodes for Li-ion batteries, *Nano Lett.*, 2009, 9(2): 612
25. C. K. Chan, R. Ruffo, S. S. Hong, and Y. Cui, Surface chemistry and morphology of the solid electrolyte interphase on silicon nanowire lithium-ion battery anodes, *J. Power Sources*, 2009, 189(2): 1132
26. R. Ruffo, S. S. Hong, C. K. Chan, R. A. Huggins, and Y. Cui, Impedance analysis of silicon nanowire lithium ion battery anodes, *J. Phys. Chem. C*, 2009, 113(26): 11390
27. C. K. Chan, R. Ruffo, S. S. Hong, R. A. Huggins, and Y. Cui, Structural and electrochemical study of the reaction

of lithium with silicon nanowires, *J. Power Sources*, 2009, 189(1): 34

28. S. Misra, N. Liu, J. Nelson, S. S. Hong, Y. Cui, and M. F. Toney, *In situ* X-ray diffraction studies of (de)lithiation mechanism in silicon nanowire anodes, *ACS Nano*, 2012, 6(6): 5465
29. J. W. Choi, J. McDonough, S. Jeong, J. S. Yoo, C. K. Chan, and Y. Cui, Stepwise nanopore evolution in one-dimensional nanostructures, *Nano Lett.*, 2010, 10(4): 1409
30. L. F. Cui, Y. Yang, C. M. Hsu, and Y. Cui, Carbon-silicon core-shell nanowires as high capacity electrode for lithium ion batteries, *Nano Lett.*, 2009, 9(9): 3370
31. L. F. Cui, R. Ruffo, C. K. Chan, H. Peng, and Y. Cui, Crystalline-amorphous coretshell silicon nanowires for high capacity and high current battery electrodes, *Nano Lett.*, 2009, 9(1): 491
32. X. Chen, K. Gerasopoulos, J. Guo, A. Brown, C. Wang, R. Ghodssi, and J. N. Culver, Virus-enabled silicon anode for lithium-ion batteries, *ACS Nano*, 2010, 4(9): 5366
33. S. Zhou, X. Liu, and D. Wang, Si/$TiSi_2$ Heteronanostructures as high-capacity anode material for li ion batteries, *Nano Lett.*, 2010, 10(3): 860
34. Y. Yao, K. Huo, L. Hu, N. Liu, J. J. Cha, M. T. McDowell, P. K. Chu, and Y. Cui, Highly conductive, mechanically robust, and electrochemically inactive TiC/C nanofiber scaffold for high-performance silicon anode batteries, *ACS Nano*, 2011, 5(10): 8346
35. H. Zhang and P. V. Braun, Three-dimensional metal scaffold supported bicontinuous silicon battery anodes, *Nano Lett.*, 2012, 12(6): 2778
36. R. Huang, X. Fan, W. Shen, and J. Zhu, Carbon-coated silicon nanowire array films for high-performance lithium-ion battery anodes, *Appl. Phys. Lett.*, 2009, 95(13): 133119
37. L. Su, Z. Zhou, and M. Ren, Core double-shell Si@SiO_2@C nanocomposites as anode materials for Li-ion batteries, *Chem. Commun.*, 2010, 46(15): 2590
38. A. Vlad, A. L. M. Reddy, A. Ajayan, N. Singh, J. F. Gohy, S. Melinte, and P. M. Ajayan, Roll up nanowire battery from silicon chips, *Proc. Natl. Acad. Sci. USA*, 2012, 109(38): 15168
39. A. Kohandehghan, P. Kalisvaart, K. Cui, M. Kupsta, E. Memarzadeh, and D. Mitlin, Silicon nanowire lithium-ion battery anodes with ALD deposited TiN coatings demonstrate a major improvement in cycling performance, *J. Mater. Chem. A*, 2013, 1: 12850
40. Y. Yao, N. Liu, M. T. McDowell, M. Pasta, and Y. Cui, Improving the cycling stability of silicon nanowire anodes with conducting polymer coatings, *Energy Environ. Sci.*, 2012, 5: 7927
41. L. Su, Y. Jing, and Z. Zhou, Li ion battery materials with core-shell nanostructures, *Nanoscale*, 2011, 3(10): 3967
42. L. F. Cui, L. Hu, H. Wu, J. W. Choi, and Y. Cui, Inorganic glue enabling high performance of silicon particles as lithium ion battery anode, *J. Electrochem. Soc.*, 2011, 158(5): A592
43. L. Hu, H. Wu, S. S. Hong, L. Cui, J. R. McDonough, S. Bohy, and Y. Cui, Si nanoparticle-decorated Si nanowire networks for Li-ion battery anodes, *Chem. Commun.*, 2011, 47(1): 367
44. A. Magasinski, P. Dixon, B. Hertzberg, A. Kvit, J. Ayala, and G. Yushin, High-performance lithium-ion anodes using a hierarchical bottom-up approach, *Nat. Mater.*, 2010, 9(4): 353
45. D. S. Jung, T. H. Hwang, S. B. Park, and J. W. Choi, Spray drying method for large-scale and high-performance silicon negative electrodes in Li-ion batteries, *Nano Lett.*, 2013, 13(5): 2092
46. A. Magasinski, B. Zdyrko, I. Kovalenko, B. Hertzberg, R. Burtovyy, C. F. Huebner, T. F. Fuller, I. Luzinov, and G. Yushin, Toward efficient binders for Li-ion battery Si-based anodes: Polyacrylic acid, *ACS Appl. Mater. Interfaces*, 2010, 2(11): 3004
47. I. Kovalenko, B. Zdyrko, A. Magasinski, B. Hertzberg, Z. Milicev, R. Burtovyy, I. Luzinov, and G. Yushin, A major constituent of brown algae for use in high-capacity Li-ion batteries, *Science*, 2011, 334(6052): 75
48. G. Liu, S. Xun, N. Vukmirovic, X. Song, P. Olalde-Velasco, H. Zheng, V. S. Battaglia, L. Wang, and W. Yang, Polymers with tailored electronic structure for high capacity lithium battery electrodes, *Adv. Mater.*, 2011, 23(40): 4679
49. H. Wu, G. Yu, L. Pan, N. Liu, M. T. McDowell, Z. Bao, and Y. Cui, Stable Li-ion battery anodes by *in-situ* polymerization of conducting hydrogel to conformally coat silicon nanoparticles, *Nat. Commun.*, 2013, 4: 1943
50. M. H. Park, M. G. Kim, J. Joo, K. Kim, J. Kim, S. Ahn, Y. Cui, and J. Cho, Silicon nanotube battery anodes, *Nano Lett.*, 2009, 9(11): 3844
51. T. Song, J. Xia, J. H. Lee, D. H. Lee, M. S. Kwon, J. M. Choi, J. Wu, S. K. Doo, H. Chang, W. I. Park, D. S. Zang, H. Kim, Y. Huang, K. C. Hwang, J. A. Rogers, and U. Paik, Arrays of sealed silicon nanotubes as anodes for lithium ion batteries, *Nano Lett.*, 2010, 10(5): 1710
52. Y. Yao, M. T. McDowell, I. Ryu, H. Wu, N. Liu, L. Hu, W. D. Nix, and Y. Cui, Interconnected silicon hollow nanospheres for lithium-ion battery anodes with long cycle life, *Nano Lett.*, 2011, 11(7): 2949
53. M. H. Park, Y. Cho, K. Kim, J. Kim, M. Liu, and J. Cho, Germanium nanotubes prepared by using the Kirkendall effect as anodes for high-rate lithium batteries, *Angew. Chem. Int. Ed.*, 2011, 123(41): 9821
54. S. Han, B. Jang, T. Kim, S. M. Oh, and T. Hyeon, Simple synthesis of hollow tin dioxide microspheres and their application to lithium-ion battery anodes, *Adv. Funct. Mater.*, 2005, 15(11): 1845
55. X. W. Lou, Y. Wang, C. Yuan, J. Y. Lee, and L. A. Archer, Template-free synthesis of SnO_2 hollow nanostructures with

high lithium storage capacity, *Adv. Mater.*, 2006, 18(17): 2325

56. H. Kim, B. Han, J. Choo, and J. Cho, Three-dimensional porous silicon particles for use in high-performance lithium secondary batteries, *Angew. Chem. Int. Ed.*, 2008, 120(52): 10305
57. Y. Yu, L. Gu, C. Zhu, S. Tsukimoto, P. A. van Aken, and J. Maier, Reversible storage of lithium in silver-coated three-dimensional macroporous silicon, *Adv. Mater.*, 2010, 22(20): 2247
58. J. Cho, Porous Si anode materials for lithium rechargeable batteries, *J. Mater. Chem.*, 2010, 20(20): 4009
59. H. Jia, P. Gao, J. Yang, J. Wang, Y. Nuli, and Z. Yang, Novel three-dimensional mesoporous silicon for high power lithium-ion battery anode material, *Adv. Energy Mater.*, 2011, 1(6): 1036
60. D. Chen, X. Mei, G. Ji, M. Lu, J. Xie, J. Lu, and J. Y. Lee, Reversible lithium-ion storage in silver-treated nanoscale hollow porous silicon particles, *Angew. Chem. Int. Ed.*, 2012, 51(10): 2409
61. J. Zhu, C. Gladden, N. Liu, Y. Cui, and X. Zhang, Nanoporous silicon networks as anodes for lithium ion batteries, *Phys. Chem. Chem. Phys.*, 2013, 15(2): 440
62. M. Ge, J. Rong, X. Fang, and C. Zhou, Porous doped silicon nanowires for lithium ion battery anode with long cycle life, *Nano Lett.*, 2012, 12(5): 2318
63. Z. Bao, M. R. Weatherspoon, S. Shian, Y. Cai, P. D. Graham, S. M. Allan, G. Ahmad, M. B. Dickerson, B. C. Church, Z. Kang, H. W. III Abernathy, C. J. Summers, M. Liu, and K. H. Sandhage, Chemical reduction of three-dimensional silica micro-assemblies into microporous silicon replicas, *Nature*, 2007, 446(7132): 172
64. W. Stöber, A. Fink, and E. Bohn, Controlled growth of monodisperse silica spheres in the micron size range, *J. Colloid Interface Sci.*, 1968, 26(1): 62
65. D. Zhao, J. Feng, Q. Huo, N. Melosh, G. H. Fredrickson, B. F. Chmelka, and G. D. Stucky, Triblock copolymer syntheses of mesoporous silica with periodic 50 to 300 angstrom pores, *Science*, 1998, 279(5350): 548
66. C. O. Tuck, E. Pérez, I. T. Horváth, R. A. Sheldon, and M. Poliakoff, Valorization of biomass: Deriving more value from waste, *Science*, 2012, 337(6095): 695
67. N. Liu, K. Huo, M. T. McDowell, J. Zhao, and Y. Cui, Rice husks as a sustainable source of nanostructured silicon for high performance Li-ion battery anodes, *Sci. Rep.*, 2013, 3: 1919
68. A. Xing, S. Tian, H. Tang, D. Losic, and Z. Bao, Mesoporous silicon engineered by the reduction of biosilica from rice husk as a high-performance anode for lithium-ion batteries, *RSC Adv.*, 2013, 3(26): 10145
69. D. S. Jung, M. H. Ryou, Y. J. Sung, S. B. Park, and J. W. Choi, Recycling rice husks for high-capacity lithium battery anodes, *Proc. Natl. Acad. Sci. USA*, 2013, 110(30): 12229
70. R. Yi, F. Dai, M. L. Gordin, S. Chen, and D. Wang, Micro-sized Si-C composite with interconnected nanoscale building blocks as high-performance anodes for practical application in lithium-ion batteries, *Adv. Energy Mater.*, 2013, 3(3): 295
71. K. Xu, Nonaqueous liquid electrolytes for lithium-based rechargeable batteries, *Chem. Rev.*, 2004, 104(10): 4303
72. P. Verma, P. Maire, and P. Novák, A review of the features and analyses of the solid electrolyte interphase in Li-ion batteries, *Electrochim. Acta*, 2010, 55(22): 6332
73. D. Aurbach, Review of selected electrode-solution interactions which determine the performance of Li and Li ion batteries, *J. Power Sources*, 2000, 89(2): 206
74. N. Liu, L. Hu, M. T. McDowell, A. Jackson, and Y. Cui, Prelithiated silicon nanowires as an anode for lithium ion batteries, *ACS Nano*, 2011, 5(8): 6487
75. V. Etacheri, O. Haik, Y. Goffer, G. A. Roberts, I. C. Stefan, R. Fasching, and D. Aurbach, Effect of fluoroethylene carbonate (FEC) on the performance and surface chemistry of Si-nanowire Li-ion battery anodes, *Langmuir*, 2012, 28(1): 965
76. V. Etacheri, U. Geiger, Y. Gofer, G. A. Roberts, I. C. Stefan, R. Fasching, and D. Aurbach, Exceptional electrochemical performance of Si-nanowires in 1,3-dioxolane solutions: A surface chemical investigation, *Langmuir*, 2012, 28(14): 6175
77. N. Liu, H. Wu, M. T. McDowell, Y. Yao, C. Wang, and Y. Cui, A yolk-shell design for stabilized and scalable li-ion battery alloy anodes, *Nano Lett.*, 2012, 12(6): 3315
78. B. Hertzberg, A. Alexeev, and G. Yushin, Deformations in Si-Li anodes upon electrochemical alloying in nano-confined space, *J. Am. Chem. Soc.*, 2010, 132(25): 8548
79. H. Wu, G. Zheng, N. Liu, T. J. Carney, Y. Yang, and Y. Cui, Engineering empty space between Si nanoparticles for lithium-ion battery anodes, *Nano Lett.*, 2012, 12(2): 904
80. X. Li, P. Meduri, X. Chen, W. Qi, M. H. Engelhard, W. Xu, F. Ding, J. Xiao, W. Wang, C. Wang, J. G. Zhang, and J. Liu, Hollow core-shell structured porous Si-C nanocomposites for Li-ion battery anodes, *J. Mater. Chem.*, 2012, 22(22): 11014
81. B. Wang, X. Li, X. Zhang, B. Luo, Y. Zhang, and L. Zhi, Contact-engineered and void-involved silicon/carbon nanohybrids as lithium-ion-battery anodes, *Adv. Mater.*, 2013, 25(26): 3560
82. K. Karki, Y. Zhu, Y. Liu, C. F. Sun, L. Hu, Y. Wang, C. Wang, and J. Cumings, Hoop-strong nanotubes for battery electrodes, *ACS Nano*, 2013, 7(9): 8295
83. X. W. Lou, C. M. Li, and L. A. Archer, Designed synthesis of coaxial SnO_2@carbon hollow nanospheres for highly reversible lithium storage, *Adv. Mater.*, 2009, 21(24): 2536
84. J. Y. Huang, L. Zhong, C. M. Wang, J. P. Sullivan, W. Xu, L. Q. Zhang, S. X. Mao, N. S. Hudak, X. H. Liu, A. Subramanian, H. Fan, L. Qi, A. Kushima, and J. Li, *In situ*

observation of the electrochemical lithiation of a single SnO_2 nanowire electrode, *Science*, 2010, 330(6010): 1515

85. M. T. McDowell, I. Ryu, S. W. Lee, C. Wang, W. D. Nix, and Y. Cui, Studying the kinetics of crystalline silicon nanoparticle lithiation with *in situ* transmission electron microscopy, *Adv. Mater.*, 2012, 24(45): 6034
86. Y. Yang, G. Zheng, and Y. Cui, Nanostructured sulfur cathodes, *Chem. Soc. Rev.*, 2013, 42(7): 3018
87. A. Manthiram, Y. Fu, and Y. S. Su, Challenges and prospects of lithium–sulfur batteries, *Acc. Chem. Res.*, 2013, 46(5): 1125
88. Y. V. Mikhaylik and J. R. Akridge, Polysulfide shuttle study in the Li/S battery system, *J. Electrochem. Soc.*, 2004, 151(11): A1969
89. X. L. Ji and L. F. Nazar, Advances in Li-S batteries, *J. Mater. Chem.*, 2010, 20(44): 9821
90. C. Barchasz, J. C. Lepretre, F. Alloin, and S. Patoux, New insights into the limiting parameters of the Li/S rechargeable cell, *J. Power Sources*, 2012, 199: 322
91. J. Shim, K. A. Striebel, and E. J. Cairns, The lithium/sulfur rechargeable cell, *J. Electrochem. Soc.*, 2002, 149(10): A1321
92. X. Ji, K. T. Lee, and L. F. Nazar, A highly ordered nanostructured carbon-sulphur cathode for lithium-sulphur batteries, *Nat. Mater.*, 2009, 8(6): 500
93. N. Jayaprakash, J. Shen, S. S. Moganty, A. Corona, and L. A. Archer, Porous hollow carbon@sulfur composites for high-power lithium-sulfur batteries, *Angew. Chem. Int. Ed.*, 2011, 50(26): 5904
94. J. Kim, D. J. Lee, H. G. Jung, Y. K. Sun, J. Hassoun, and B. Scrosati, An advanced lithium-sulfur battery, *Adv. Funct. Mater.*, 2013, 23(8): 1076
95. J. Guo, Y. Xu, and C. Wang, Sulfur-impregnated disordered carbon nanotubes cathode for lithium-sulfur batteries, *Nano Lett.*, 2011, 11(10): 4288
96. L. Ji, M. Rao, S. Aloni, L. Wang, E. J. Cairns, and Y. Zhang, Porous carbon nanofiber-sulfur composite electrodes for lithium/sulfurcells, *Energy Environ. Sci.*, 2011, 4: 5053
97. C. Zu, Y. Fu, and A. Manthiram, Highly reversible Li/dissolved polysulfide batteries with binder-free carbon nanofiber electrodes, *J. Mater. Chem. A*, 2013, 1(35): 10362
98. R. Elazari, G. Salitra, A. Garsuch, A. Panchenko, and D. Aurbach, Sulfur-impregnated activated carbon fiber cloth as a binder-free cathode for rechargeable Li-S batteries, *Adv. Mater.*, 2011, 23(47): 5641
99. Y. S. Su and A. Manthiram, Lithium-sulfur batteries with a microporous carbon paper as a bifunctional interlayer, *Nat. Commun.*, 2012, 3: 1166
100. B. Zhang, C. Lai, Z. Zhou, and X. P. Gao, Preparation and electrochemical properties of sulfur-acetylene black composites as cathode materials, *Electrochim. Acta*, 2009, 54(14): 3708
101. C. Lai, X. P. Gao, B. Zhang, T. Y. Yan, and Z. Zhou, Synthesis and Electrochemical Performance of Sulfur/Highly Porous Carbon Composites, *J. Phys. Chem. C*, 2009, 113(11): 4712
102. L. Ji, M. Rao, H. Zheng, L. Zhang, Y. Li, W. Duan, J. Guo, E. J. Cairns, and Y. Zhang, Graphene oxide as a sulfur immobilizer in high performance lithium/sulfur cells, *J. Am. Chem. Soc.*, 2011, 133(46): 18522
103. H. Wang, Y. Yang, Y. Liang, J. T. Robinson, Y. Li, A. Jackson, Y. Cui, and H. Dai, Graphene-wrapped sulfur particles as a rechargeable lithium-sulfur battery cathode material with high capacity and cycling stability, *Nano Lett.*, 2011, 11(7): 2644
104. G. Zheng, Y. Yang, J. J. Cha, S. S. Hong, and Y. Cui, Hollow carbon nanofiber-encapsulated sulfur cathodes for high specific capacity rechargeable lithium batteries, *Nano Lett.*, 2011, 11(10): 4462
105. G. Zheng, Q. Zhang, J. J. Cha, Y. Yang, W. Li, Z. W. Seh, and Y. Cui, Amphiphilic surface modification of hollow carbon nanofibers for improved cycle life of lithium sulfur batteries, *Nano Lett.*, 2013, 13(3): 1265
106. H. Yao, G. Zheng, W. Li, M. T. McDowell, Z. W. Seh, N. Liu, Z. Lu, and Y. Cui, Crab shells as sustainable templates from nature for nanostructured battery electrodes, *Nano Lett.*, 2013, 13(7): 3385
107. Y. Yang, G. Yu, J. J. Cha, H. Wu, M. Vosgueritchian, Y. Yao, Z. Bao, and Y. Cui, Improving the performance of lithium-sulfur batteries by conductive polymer coating, *ACS Nano*, 2011, 5(11): 9187
108. X. Ji, S. Evers, R. Black, and L. F. Nazar, Stabilizing lithium-sulphur cathodes using polysulphide reservoirs, *Nat. Commun.*, 2011, 2: 325
109. S. Evers, T. Yim, and L. F. Nazar, Understanding the nature of absorption/adsorption in nanoporous polysulfide sorbents for the Li-S battery, *J. Phys. Chem. C*, 2012, 116(37): 19653
110. J. Schuster, G. He, B. Mandlmeier, T. Yim, K. T. Lee, T. Bein, and L. F. Nazar, Spherical ordered mesoporous carbon nanoparticles with high porosity for lithium-sulfur batteries, *Angew. Chem. Int. Ed.*, 2012, 51(15): 3591
111. J. Nelson, S. Misra, Y. Yang, A. Jackson, Y. Liu, H. Wang, H. Dai, J. C. Andrews, Y. Cui, and M. F. Toney, In Operando X-ray diffraction and transmission X-ray microscopy of lithium sulfur batteries, *J. Am. Chem. Soc.*, 2012, 134(14): 6337
112. Z. W. Seh, W. Li, J. J. Cha, G. Zheng, Y. Yang, M. T. McDowell, P. C. Hsu, and Y. Cui, Sulphur-TiO_2 yolk-shell nanoarchitecture with internal void space for long-cycle lithium-sulphur batteries, *Nat. Commun.*, 2013, 4: 1331
113. W. Li, G. Zheng, Y. Yang, Z. W. Seh, N. Liu, and Y. Cui, High-performance hollow sulfur nanostructured battery cathode through a scalable, room temperature, one-step, bottom-up approach, *Proc. Natl. Acad. Sci. USA*, 2013, 110(18): 7148

114. R. Demir-Cakan, M. Morcrette, F. Nouar, C. Davoisne, T. Devic, D. Gonbeau, R. Dominko, C. Serre, G. Férey, and J. M. Tarascon, Cathode composites for Li-S batteries via the use of oxygenated porous architectures, *J. Am. Chem. Soc.*, 2011, 133(40): 16154

115. L. Xiao, Y. Cao, J. Xiao, B. Schwenzer, M. H. Engelhard, L. V. Saraf, Z. Nie, G. J. Exarhos, and J. Liu, A soft approach to encapsulate sulfur: Polyaniline nanotubes for lithium-sulfur batteries with long cycle life, *Adv. Mater.*, 2012, 24(9): 1176

116. Y. Fu and A. Manthiram, Core-shell structured sulfur-polypyrrole composite cathodes for lithium–sulfur batteries, *RSC Adv.*, 2012, 2: 5927

117. H. Chen, W. Dong, J. Ge, C. Wang, X. Wu, W. Lu, and L. Chen, Ultrafine sulfur nanoparticles in conducting polymer shell as cathode materials for high performance lithium/sulfur batteries, *Sci. Rep.*, 2013, 3: 1910

118. Y. Bouligand, Twisted fibrous arrangements in biological materials and cholesteric mesophases, *Tissue Cell*, 1972, 4(2): 189

119. R. Roer and R. Dillaman, The structure and calcification of the crustacean cuticle, *Am. Zool.*, 1984, 24: 893

120. M. M. Giraud-Guille, Plywood structures in nature, *Curr. Opin. Solid State Mater. Sci.*, 1998, 3(3): 221

121. P. Y. Chen, A. Y. M. Lin, J. McKittrick, and M. A. Meyers, Structure and mechanical properties of crab exoskeletons, *Acta Biomater.*, 2008, 4(3): 587

122. N. Fujita, M. Asai, T. Yamashita, and S. Shinkai, Sol-gel transcription of silica-based hybrid nanostructures using poly(*N*-vinylpyrrolidone)-coated [60]fullerene, single-walled carbon nanotube and block copolymer templates, *J. Mater. Chem.*, 2004, 14(14): 2106

123. M. J. O'Connell, P. Boul, L. M. Ericson, C. Huffman, Y. Wang, E. Haroz, C. Kuper, J. Tour, K. D. Ausman, and R. E. Smalley, Reversible water-solubilization of single-walled carbon nanotubes by polymer wrapping, *Chem. Phys. Lett.*, 2001, 342(3–4): 265

124. J. Hassoun and B. Scrosati, A high-performance polymer tin sulfur lithium ion battery, *Angew. Chem. Int. Ed.*, 2010, 49(13): 2371

125. M. Nagao, A. Hayashi, and M. Tatsumisago, High-capacity Li_2S–nanocarbon composite electrode for all-solid-state rechargeable lithium batteries, *J. Mater. Chem.*, 2012, 22(19): 10015

126. K. Cai, M. K. Song, E. J. Cairns, and Y. Zhang, Nanostructured Li_2S-C composites as cathode material for high-energy lithium/sulfur batteries, *Nano Lett.*, 2012, 12(12): 6474

127. J. Guo, Z. Yang, Y. Yu, H. D. Abruña, and L. A. Archer, Lithium-sulfur battery cathode enabled by lithium-nitrile interaction, *J. Am. Chem. Soc.*, 2013, 135(2): 763

128. Z. Lin, Z. Liu, N. J. Dudney, and C. Liang, Lithium superionic sulfide cathode for all-solid lithium-sulfur batteries, *ACS Nano*, 2013, 7(3): 2829

129. Y. Yang, M. T. McDowell, A. Jackson, J. J. Cha, S. S. Hong, and Y. Cui, New nanostructured Li_2S/silicon rechargeable battery with high specific energy, *Nano Lett.*, 2010, 10(4): 1486

130. Y. Yang, G. Zheng, S. Misra, J. Nelson, M. F. Toney, and Y. Cui, High-capacity micrometer-sized Li_2S particles as cathode materials for advanced rechargeable lithium-ion batteries, *J. Am. Chem. Soc.*, 2012, 134(37): 15387

131. Z. W. Seh, Q. Zhang, W. Li, G. Zheng, H. Yao, and Y. Cui, Stable cycling of lithium sulfide cathodes through strong affinity with a bifunctional binder, *Chem. Sci.*, 2013, 4(9): 3673

132. A. Kraft, On the discovery and history of prussian blue, *Bull. Hist. Chem.*, 2008, 33(2): 61

133. S. I. Ohkoshi, K. I. Arai, Y. Sato, and K. Hashimoto, Humidity-induced magnetization and magnetic pole inversion in a cyano-bridged metal assembly, *Nat. Mater.*, 2004, 3(12): 857

134. T. Matsuda, J. Kim, and Y. Moritomo, Symmetry switch of cobalt ferrocyanide framework by alkaline cation exchange, *J. Am. Chem. Soc.*, 2010, 132(35): 12206

135. E. Coronado, M. C. Giménez-López, G. Levchenko, F. M. Romero, V. García-Baonza, A. Milner, and M. Paz-Pasternak, Pressure-tuning of magnetism and linkage isomerism in iron(II) hexacyanochromate, *J. Am. Chem. Soc.*, 2005, 127(13): 4580

136. S. Margadonna, K. Prassides, and A. N. Fitch, Zero thermal expansion in a Prussian Blue analogue, *J. Am. Chem. Soc.*, 2004, 126(47): 15390

137. S. S. Kaye and J. R. Long, Hydrogen storage in the dehydrated prussian blue analogues $M_3[Co(CN)_6]_2$ (M = Mn, Fe, Co, Ni, Cu, Zn), *J. Am. Chem. Soc.*, 2005, 127(18): 6506

138. K. Hashimoto and H. Ohkoshi, Design of novel magnets using Prussian blue analogues, *Phil. Trans. R. Soc. Lond. A*, 1999, 357(1762): 2977

139. T. Mallah, A. Marvilliers, and E. Rivière, From ferromagnets to high-spin molecules: The role of the organic ligands, *Phil. Trans. R. Soc. Lond. A*, 1999, 357(1762): 3139

140. M. Verdaguer, A. Bleuzen, V. Marvaud, J. Vaissermann, M. Seuleiman, C. Desplanches, A. Scuiller, C. Train, R. Garde, G. Gelly, C. Lomenech, I. Rosenman, P. Veillet, C. Cartier, and F. Villain, Molecules to build solids: High T_c molecule-based magnets by design and recent revival of cyano complexes chemistry, *Coord. Chem. Rev.*, 1999, 190–192: 1023

141. A. A. Karyakin, Prussian blue and its analogues: Electrochemistry and analytical applications, *Electroanalysis*, 2001, 13(10): 813

142. T. Matsuda, J. Kim, K. Ohoyama, and Y. Moritomo, Universal thermal response of the Prussian blue lattice, *Phys. Rev. B*, 2009, 79(17): 172302

143. A. Ludi and H. Güdel, Inorganic Chemistry, Berlin/ Heidelberg: Springer, 1973: 1

144. H. J. Buser, D. Schwarzenbach, W. Petter, and A. Ludi, The crystal structure of Prussian blue: $Fe_4[Fe(CN)_6]_3.xH_2O$, *Inorg. Chem.*, 1977, 16(11): 2704

145. F. Herren, P. Fischer, A. Ludi, and W. Hälg, Neutron diffraction study of Prussian blue, $Fe_4[Fe(CN)_6]_3.xH_2O$. Location of water molecules and long-range magnetic order, *Inorg. Chem.*, 1980, 19(4): 956

146. P. Bhatt, N. Thakur, M. D. Mukadam, S. S. Meena, and S. M. Yusuf, Evidence for the existence of oxygen clustering and understanding of structural disorder in prussian blue analogues molecular magnet $M_{15}[Cr(CN)_6]\cdot zH_2O$ (M = Fe and Co): Reverse Monte Carlo simulation and neutron diffraction study, *J. Phys. Chem. C*, 2013, 117(6): 2676

147. C. D. Wessells, R. A. Huggins, and Y. Cui, Copper hexacyanoferrate battery electrodes with long cycle life and high power, *Nat. Commun.*, 2011, 2: 550

148. D. E. Stilwell, K. H. Park, and M. H. Miles, Electrochemical studies of the factors influencing the cycle stability of Prussian blue films, *J. Appl. Electrochem.*, 1992, 22(4): 325

149. T. Oi, Electrochromic materials, *Annu. Rev. Mater. Sci.*, 1986, 16(1): 185

150. K. Itaya, T. Ataka, and S. Toshima, Spectroelectrochemistry and electrochemical preparation method of Prussian blue modified electrodes, *J. Am. Chem. Soc.*, 1982, 104(18): 4767

151. F. Scholz and A. Dostal, The formal potentials of solid metal hexacyanometalates, *Angew. Chem. Int. Ed. Engl.*, 1996, 34(2324): 2685

152. N. Imanishi, T. Morikawa, J. Kondo, Y. Takeda, O. Yamamoto, N. Kinugasa, and T. Yamagishi, Lithium intercalation behavior into iron cyanide complex as positive electrode of lithium secondary battery, *J. Power Sources*, 1999, 79(2): 215

153. D. Asakura, C. H. Li, Y. Mizuno, M. Okubo, H. S. Zhou, and D. R. Talham, Bimetallic cyanide-bridged coordination polymers as lithium ion cathode materials: Core-shell nanoparticles with enhanced cyclability, *J. Am. Chem. Soc.*, 2013, 135(7): 2793

154. X. J. Wang, F. Krumeich, and R. Nesper, Nanocomposite of manganese ferrocyanide and graphene: A promising cathode material for rechargeable lithium ion batteries, *Electrochem. Commun.*, 2013, 34: 246

155. N. Imanishi, T. Morikawa, J. Kondo, R. Yamane, Y. Takeda, O. Yamamoto, H. Sakaebe, and M. Tabuchi, Lithium intercalation behavior of iron cyanometallates, *J. Power Sources*, 1999, 81–82: 530

156. M. Takachi, Y. Kurihara, and Y. Moritomo, Channel size dependence of Li^+ insertion/extraction in nanoporous hexacyanoferrates, *J. Mater. Sci. Eng. B*, 2012, 2(8): 452

157. M. Okubo and I. Honma, Ternary metal Prussian blue analogue nanoparticles as cathode materials for Li-ion batteries, *Dalton Trans.*, 2013, 42(45): 15881

158. M. Takachi, T. Matsuda, and Y. Moritomo, Structural, electronic, and electrochemical properties of $Li_xO[Fe(CN)_6]_{0.90}\cdot 2.9H_2O$, *Jpn. J. Appl. Phys.*, 2013, 52: 044301

159. L. Wang, Y. H. Lu, J. Liu, M. W. Xu, J. G. Cheng, D. W. Zhang, and J. B. Goodenough, A superior low-cost cathode for a Na-ion battery, *Angew. Chem. Int. Ed.*, 2013, 52(7): 1964

160. Y. Lu, L. Wang, J. Cheng, and J. B. Goodenough, Prussian blue: A new framework of electrode materials for sodium batteries, *Chem. Commun.*, 2012, 48(52): 6544

161. H. Lee, Y. I. Kim, J. K. Park, and J. W. Choi, Sodium zinc hexacyanoferrate with a well-defined open framework as a positive electrode for sodium ion batteries, *Chem. Commun.*, 2012, 48(67): 8416

162. T. Matsuda, M. Takachi, and Y. Moritomo, A sodium manganese ferrocyanide thin film for Na-ion batteries, *Chem. Commun.*, 2013, 49(27): 2750

163. M. Takachi, T. Matsuda, and Y. Moritomo, Cobalt hexacyanoferrate as cathode material for Na^+ secondary battery, *Appl. Phys. Express*, 2013, 6(2): 025802

164. W. Li, J. R. Dahn, and D. S. Wainwright, Rechargeable lithium batteries with aqueous electrolytes, *Science*, 1994, 264(5162): 1115

165. Y. Mizuno, M. Okubo, D. Asakura, T. Saito, E. Hosono, Y. Saito, K. Oh-ishi, T. Kudo, and H. Zhou, Impedance spectroscopic study on interfacial ion transfers in cyanide-bridged coordination polymer electrode with organic electrolyte, *Electrochim. Acta*, 2012, 63: 139

166. Y. Mizuno, M. Okubo, E. Hosono, T. Kudo, H. Zhou, and K. Oh-ishi, Suppressed activation energy for interfacial charge transfer of a Prussian blue analog thin film electrode with hydrated ions (Li^+, Na^+, and Mg^{2+}), *J. Phys. Chem. C*, 2013, 117(21): 10877

167. S. I. Ohkoshi, K. Nakagawa, K. Tomono, K. Imoto, Y. Tsunobuchi, and H. Tokoro, High proton conductivity in prussian blue analogues and the interference effect by magnetic ordering, *J. Am. Chem. Soc.*, 2010, 132(19): 6620

168. Y. Moritomo, T. Matsuda, Y. Kurihara, and J. Kim, Cubic-rhombohedral structural phase transition in $Na_{1.32}Mn[Fe(CN)_6]_{0.83}\cdot 3.6H_2O$, *J. Phys. Soc. Jpn.*, 2011, 80(7): 074608

169. C. D. Wessells, M. T. McDowell, S. V. Peddada, M. Pasta, R. A. Huggins, and Y. Cui, Tunable reaction potentials in open framework nanoparticle battery electrodes for grid-scale energy storage, *ACS Nano*, 2012, 6(2): 1688

170. R. Chen, H. Tanaka, T. Kawamoto, M. Asai, C. Fukushima, H. Na, M. Kurihara, M. Watanabe, M. Arisaka, and T. Nankawa, Selective removal of cesium ions from wastewater using copper hexacyanoferrate nanofilms in an electrochemical system, *Electrochim. Acta*, 2013, 87: 119

171. C. D. Wessells, S. V. Peddada, M. T. McDowell, R. A. Huggins, and Y. Cui, The effect of insertion species on nanostruc-

tured open framework hexacyanoferrate battery electrodes, *J. Electrochem. Soc.*, 2012, 159(2): A98

172. C. D. Wessells, S. V. Peddada, R. A. Huggins, and Y. Cui, Nickel hexacyanoferrate nanoparticle electrodes for aqueous sodium and potassium ion batteries, *Nano Lett.*, 2011, 11(12): 5421

173. M. Pasta, C. D. Wessells, R. A. Huggins, and Y. Cui, A high-rate and long cycle life aqueous electrolyte battery for grid-scale energy storage, *Nat. Commun.*, 2012, 3: 1149

174. R. Klenze, B. Kanellakopulos, G. Trageser, and H. H. Eysel, Manganese hexacyanomanganate: Magnetic interactions via cyanide in a mixed valence Prussian blue type compound, *J. Chem. Phys.*, 1980, 72(11): 5819

175. J. H. Her, P. W. Stephens, C. M. Kareis, J. G. Moore, K. S. Min, J. W. Park, G. Bali, B. S. Kennon, and J. S. Miller, Anomalous non-Prussian blue structures and magnetic ordering of $K_2Mn^{II}[Mn^{II}(CN)_6]$ and $Rb_2Mn^{II}[Mn^{II}(CN)_6]$, *Inorg. Chem.*, 2010, 49(4): 1524

176. M. Pasta, C. D. Wessells, N. Liu, J. Nelson, M. T. McDowell, R. A. Huggins, M. F. Toney, and Y. Cui, Full open-framework batteries for stationary energy storage, *Nat. Commun.*, DOI: 10.1038/ncomms4007, 2014

177. R. Y. Wang, C. D. Wessells, R. A. Huggins, and Y. Cui, Highly reversible open framework nanoscale electrodes for divalent ion batteries, *Nano Lett.*, 2013, 13(11): 5748

178. F. La Mantia, M. Pasta, H. D. Deshazer, B. E. Logan, and Y. Cui, Batteries for efficient energy extraction from a water salinity difference, *Nano Lett.*, 2011, 11(4): 1810

179. M. Pasta, C. D. Wessells, Y. Cui, and F. La Mantia, A desalination battery, *Nano Lett.*, 2012, 12(2): 839

180. M. Pasta, A. Battistel, and F. La Mantia, Batteries for lithium recovery from brines, *Energy Environ. Sci.*, 2012, 5(11): 9487

181. P. J. Hall, M. Mirzaeian, S. I. Fletcher, F. B. Sillars, A. J. R. Rennie, G. O. Shitta-Bey, G. Wilson, A. Cruden, and R. Carter, Energy storage in electrochemical capacitors: designing functional materials to improve performance, *Energy Environ. Sci.*, 2010, 3(9): 1238

182. M. Winter and R. J. Brodd, What are batteries, fuel cells, and supercapacitors? *Chem. Rev.*, 2004, 104(10): 4245

183. J. R. Miller and P. Simon, Electrochemical capacitors for energy management, *Science*, 2008, 321(5889): 651

184. P. Simon and Y. Gogotsi, Materials for electrochemical capacitors, *Nat. Mater.*, 2008, 7(11): 845

185. V. Subramanian, S. C. Hall, P. H. Smith, and B. Rambabu, Mesoporous anhydrous RuO_2 as a supercapacitor electrode material, *Solid State Ion.*, 2004, 175(1–4): 511

186. C. C. Hu, K. H. Chang, M. C. Lin, and Y. T. Wu, Design and tailoring of the nanotubular arrayed architecture of hydrous RuO_2 for next generation supercapacitors, *Nano Lett.*, 2006, 6(12): 2690

187. H. Y. Lee and J. B. Goodenough, Supercapacitor behavior with KCl electrolyte, *J. Solid State Chem.*, 1999, 144(1): 220

188. A. Rudge, J. Davey, I. Raistrick, S. Gottesfeld, and J. P. Ferraris, Conducting polymers as active materials in electrochemical capacitors, *J. Power Sources*, 1994, 47(1–2): 89

189. L. Hu and Y. Cui, Energy and environmental nanotechnology in conductive paper and textiles, *Energy Environ. Sci.*, 2012, 5(4): 6423

190. C. Niu, E. K. Sichel, R. Hoch, D. Moy, and H. Tennent, High power electrochemical capacitors based on carbon nanotube electrodes, *Appl. Phys. Lett.*, 1997, 70(11): 1480

191. M. Kaempgen, C. K. Chan, J. Ma, Y. Cui, and G. Gruner, Printable thin film supercapacitors using single-walled carbon nanotubes, *Nano Lett.*, 2009, 9(5): 1872

192. L. Hu, J. W. Choi, Y. Yang, S. Jeong, F. La Mantia, L. F. Cui, and Y. Cui, Highly conductive paper for energy-storage devices, *Proc. Natl. Acad. Sci. USA*, 2009, 106(51): 21490

193. M. Pasta, F. La Mantia, L. Hu, H. Deshazer, and Y. Cui, Aqueous supercapacitors on conductive cotton, *Nano Res.*, 2010, 3(6): 452

194. L. Hu, M. Pasta, F. L. Mantia, L. Cui, S. Jeong, H. D. Deshazer, J. W. Choi, S. M. Han, and Y. Cui, Stretchable, porous, and conductive energy textiles, *Nano Lett.*, 2010, 10(2): 708

195. X. Xie, G. Yu, N. Liu, Z. Bao, C. S. Criddle, and Y. Cui, Graphene–sponges as high-performance low-cost anodes for microbial fuel cells, *Energy Environ. Sci.*, 2012, 5: 6862

196. L. Hu, H. Wu, and Y. Cui, Printed energy storage devices by integration of electrodes and separators into single sheets of paper, *Appl. Phys. Lett.*, 2010, 96(18): 183502

197. G. Zheng, L. Hu, H. Wu, X. Xie, and Y. Cui, Paper supercapacitors by a solvent-free drawing method, *Energy Environ. Sci.*, 2011, 4(9): 3368

198. Z. S. Wu, G. Zhou, L. C. Yin, W. Ren, F. Li, and H. M. Cheng, Graphene/metal oxide composite electrode materials for energy storage, *Nano Energy*, 2012, 1(1): 107

199. G. Yu, X. Xie, L. Pan, Z. Bao, and Y. Cui, Hybrid nanostructured materials for high-performance electrochemical capacitors, *Nano Energy*, 2013, 2(2): 213

200. X. Lang, A. Hirata, T. Fujita, and M. Chen, Nanoporous metal/oxide hybrid electrodes for electrochemical supercapacitors, *Nat. Nanotechnol.*, 2011, 6(4): 232

201. L. Hu, W. Chen, X. Xie, N. Liu, Y. Yang, H. Wu, Y. Yao, M. Pasta, H. N. Alshareef, and Y. Cui, Symmetrical MnO_2-carbon nanotube-textile nanostructures for wearable pseudocapacitors with high mass loading, *ACS Nano*, 2011, 5(11): 8904

202. W. Chen, R. B. Rakhi, L. Hu, X. Xie, Y. Cui, and H. N. Alshareef, High-performance nanostructured supercapacitors on a sponge, *Nano Lett.*, 2011, 11(12): 5165

203. G. Yu, L. Hu, M. Vosgueritchian, H. Wang, X. Xie, J. R. McDonough, X. Cui, Y. Cui, and Z. Bao, Solution-processed graphene/MnO_2 nanostructured textiles for high-performance electrochemical capacitors, *Nano Lett.*, 2011, 11(7): 2905

204. G. Yu, L. Hu, N. Liu, H. Wang, M. Vosgueritchian, Y. Yang, Y. Cui, and Z. Bao, Enhancing the supercapacitor performance of graphene/MnO_2 nanostructured electrodes by conductive wrapping, *Nano Lett.*, 2011, 11(10): 4438

205. N. A. Peppas, J. Z. Hilt, A. Khademhosseini, and R. Langer, Hydrogels in biology and medicine: From molecular principles to bionanotechnology, *Adv. Mater.*, 2006, 18(11): 1345

206. A. Guiseppi-Elie, Electroconductive hydrogels: Synthesis, characterization and biomedical applications, *Biomaterials*, 2010, 31(10): 2701

207. R. A. Green, S. Baek, L. A. Poole-Warren, and P. J. Martens, Conducting polymer-hydrogels for medical electrode applications, *Sci. Technol. Adv. Mater.*, 2010, 11(1): 014107

208. S. Ghosh, J. Rasmusson, and O. Inganäs, Supramolecular self-assembly for enhanced conductivity in conjugated polymer blends: Ionic crosslinking in blends of poly(3,4-ethylenedioxythiophene)-poly(styrenesulfonate) and poly(vinylpyrrolidone), *Adv. Mater.*, 1998, 10(14): 1097

209. S. Ghosh and O. Inganäs, Conducting polymer hydrogels as 3D electrodes: Applications for supercapacitors, *Adv. Mater.*, 1999, 11(14): 1214

210. N. Mano, J. E. Yoo, J. Tarver, Y. L. Loo, and A. Heller, An electron-conducting cross-linked polyaniline-based redox hydrogel, formed in one step at pH 7.2, wires glucose oxidase, *J. Am. Chem. Soc.*, 2007, 129(22): 7006

211. L. Pan, G. Yu, D. Zhai, H. R. Lee, W. Zhao, N. Liu, H. Wang, B. C. K. Tee, Y. Shi, Y. Cui, and Z. Bao, Hierarchical nanostructured conducting polymer hydrogel with high electrochemical activity, *Proc. Natl. Acad. Sci. USA*, 2012, 109(24): 9287

212. Y. Zhao, B. Liu, L. Pan, and G. Yu, 3D nanostructured conductive polymer hydrogels for high-performance electrochemical devices, *Energy Environ. Sci.*, 2013, 6(10): 2856